JOURNAL OF GEOPHYSICAL RESEARCH, VOL. 101, NO. B3, PAGES 6233–6253, MARCH 10, 1996

Holocene paleoseismicity, temporal clustering, and probabilities of future large (M > 7) earthquakes on the Wasatch fault zone, Utah

J. P. McCalpin
GEO-HAZ Consulting, Incorporated, Estes Park, Colorado

S. P. Nishenko[1]
U.S. Geological Survey, National Earthquake Information Center, Denver, Colorado

Abstract. The chronology of M>7 paleoearthquakes on the central five segments of the Wasatch fault zone (WFZ) is one of the best dated in the world and contains 16 earthquakes in the past 5600 years with an average repeat time of 350 years. Repeat times for individual segments vary by a factor of 2, and range from about 1200 to 2600 years. Four of the central five segments ruptured between ~ 620±30 and 1230±60 calendar years B.P. The remaining segment (Brigham City segment) has not ruptured in the past 2120±100 years. Comparison of the WFZ space-time diagram of paleoearthquakes with synthetic paleoseismic histories indicates that the observed temporal clusters and gaps have about an equal probability (depending on model assumptions) of reflecting random coincidence as opposed to intersegment contagion. Regional seismicity suggests that for exposure times of 50 and 100 years, the probability for an earthquake of M>7 anywhere within the Wasatch Front region, based on a Poisson model, is 0.16 and 0.30, respectively. A fault-specific WFZ model predicts 50 and 100 year probabilities for a M>7 earthquake on the WFZ itself, based on a Poisson model, as 0.13 and 0.25, respectively. In contrast, segment-specific earthquake probabilities that assume quasi-periodic recurrence behavior on the Weber, Provo, and Nephi segments are less (0.01-0.07 in 100 years) than the regional or fault-specific estimates (0.25-0.30 in 100 years), due to the short elapsed times compared to average recurrence intervals on those segments. The Brigham City and Salt Lake City segments, however, have time-dependent probabilities that approach or exceed the regional and fault specific probabilities. For the Salt Lake City segment, these elevated probabilities are due to the elapsed time being approximately equal to the average late Holocene recurrence time. For the Brigham City segment, the elapsed time is significantly longer than the segment-specific late Holocene recurrence time.

Introduction

The Wasatch fault zone (WFZ) of central Utah (Figure 1) is one of the most intensively studied normal faults in the world [*Swan et al.*, 1980; *Schwartz and Coppersmith*, 1984; *Machette et al.*, 1991, 1992a, b]. Prominent fault scarps attest to late Holocene surface faulting along much of the WFZ. Radiocarbon and thermoluminescence age estimates from 65 trenches across range front scarps have established what is believed to be a complete chronology of M>7 earthquakes since 5-6 ka (ka=1000 years before present)[*Machette et al.*, 1992b]. These earthquakes are inferred to have been between M 7 and 7.5 and have been termed "characteristic earthquakes" by *Schwartz and Coppersmith* [1984]. Despite the evidence for prehistoric earthquakes, however, no earthquake larger than M 3 has been clearly associated with the WFZ in 130 years of recorded history [*Arabasz et al.*, 1992]. Although historic earthquakes as large as M 6.6 have occurred in central Utah (1934 Hansel Valley [*Shenon*, 1935]), the lack of large historic earthquakes on the WFZ itself makes forecasting larger (M>7), damaging earthquakes along the Wasatch Front problematic.

Gilbert [1884] was the first to propose that the WFZ would be the site of a future earthquake disaster. His long-term forecast, on what is now recognized as the Salt Lake City segment of the WFZ, was based on the conspicuous absence of young fault scarps in northeast Salt Lake City and the hypothesis that "any locality on the fault line of a large mountain range, which has been exempt from earthquake for a long time, is by so much nearer to the date of recurrence" [*Gilbert*, 1884, p. 52]. Our reevaluation of future earthquakes on the WFZ is based on the results of 20 years of paleoseismic studies, including trenching and numerical dating at 14 sites on the central five segments of the WFZ. We reevaluate 276 numerical ages on samples collected from WFZ trenches, compile a new space-time diagram illustrating the paleoearthquake history, and test whether the observed temporal clusters and gaps of paleoearthquakes can be distinguished

[1]Now at The Natural Hazards Center, University of Colorado, Boulder.

Paper number 95JB02851.
0148-0227/96/95JB-02851$05.00

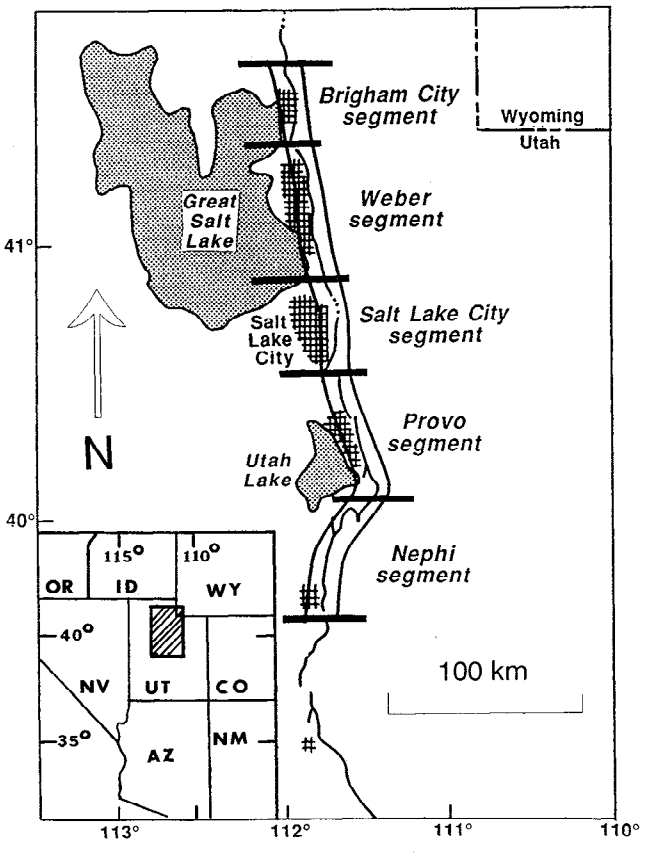

Figure 1. Location map of central Utah showing the central Wasatch fault zone. Thick horizontal lines separate the five central fault segments, as defined by *Machette et al.* [1991] (named at right). Cross hachures show major urban areas of the Wasatch Front. The surface fault trace (thin line) is adapted from *Machette et al.* [1992a], with parallel boundary lines defining each segment. Inset shows location of Figure 1 with respect to the western United States.

from random occurrences on the individual segments. Finally, recurrence intervals for the entire WFZ and individual segments are used to calculate conditional probabilities for future $M>7$ earthquakes.

Typical Stratigraphy of WFZ Exposures

To relate numerical ages to the timing of paleoearthquakes, one must first understand the stratigraphic framework typically observed in exposures of normal faults (Figure 2). After formation of a coseismic fault scarp in unconsolidated deposits, the loose material exposed in the scarp face (free face of *Wallace* [1977]) is transported to the base of the scarp and forms a colluvial wedge [*Swan et al.*, 1980; *Nash*, 1980; *Schwartz and Coppersmith*, 1984]. Based on historical fault scarps in the western United States, free faces disappear within a few years to decades after faulting (Wallace, 1977, 1980, 1984). Subsequent stages of scarp degradation are dominated by slope wash, rain splash, and creep, which lead to slope decline rather than slope retreat. Colluvium deposited under these conditions (wash-element colluvium of *Nelson* [1992]; Figure 2, units 1W, 2W) over long time periods is finer grained, better sorted, better stratified, and richer in organics than is debris-element colluvium.

The unconformity between scarp-derived colluvium and the prefaulting ground surface (on which a soil is often developed) constitutes an "event horizon" by the terminology of *Pantosti et al.* [1993] that records the occurrence of a paleoearthquake. This unconformity is time transgressive away from the scarp because laterally accreting colluvium gradually buries the prefaulting surface.

Topographic lows are common at the base of WFZ fault scarps and are filled with a combination of laterally accreting colluvium shed from the scarp (Figure 2, left and right) and vertically accreting graben deposits (Figure 2, center) of various origins (eolian sand and loess, debris flows, alluvium, marsh, and lacustrine deposits). Vertically accreting graben deposits interfinger with contemporaneous, laterally accreting colluvium near the base of the fault scarp (Figure 2). Graben deposits commonly contain more datable material (organics for ^{14}C dating, eolian deposits for thermoluminescence dating) than does scarp-derived colluvium, so tracing contacts between the graben and colluvial wedges is important in dating paleoearthquakes [e.g., *McCalpin et al.* [1994].

Unconformities often exist in the colluvial and graben fill sequences, but every unconformity may not be an event horizon. In the colluvial wedge sequence, a soil buried by coarse colluvium usually indicates renewed deposition from a free face after faulting [*Swan et al.*, 1980] and thus is usually an event horizon. In the graben, however, renewed deposition atop a soil only represents a change in the eolian, fluvial, or lacustrine depositional processes that dominate the graben. Such process changes may be caused directly by climate change or storms, or indirectly by surface faulting, which may cause drainages across the scarp to incise and induce a rapid cycle of graben deposition as streams regrade themselves. In general, unconformities that are continuous through both lateral- and vertical-accretion deposits are usually interpreted as event horizons (Figure 2, base of units 1S, 2S). Additional unconformities in the graben sequence (Figure 2, base of unit 1.5S) may reflect only climatic effects.

Distribution of Datable Material in WFZ Exposures

Organic material for ^{14}C dating is found in various forms and in various stratigraphic settings in WFZ exposures (Figure 2). Detrital charcoal and in situ burn layers (crosses in Figure 2) may be found in any deposit but are more common in finer graben deposits and wash-element colluvium than in debris-element colluvium. Thin lenses of peat or organic silt are also found in graben deposits (Fig. 2, location 7). Due to the episodic nature of fault zone sedimentation, buried soils are abundant; along the semiarid WFZ the weak A horizons of buried soils typically contain $\leq 5\%$ organic matter. Fissures formed during normal faulting are commonly filled with an organic-rich fissure fill, which is inferred to have fallen into the fissure from the surface A horizon at the time of faulting.

Thermoluminescence (TL) dating on the WFZ has been performed on fine grained sag pond deposits (both subaerial and subaqueous [*Forman et al.*, 1989]), wash-element colluvium [*Forman et al.*, 1991], and buried A horizons. Due to rapid deposition rates, debris-element colluvium is unsuitable for TL dating [*McCalpin and Forman*, 1988].

Numerical Age Database for WFZ Paleoearthquakes

For this study, we inventoried and reevaluated all 276 numerical ages (^{14}C and thermoluminescence) collected from trenches and natural exposures on the WFZ to identify those

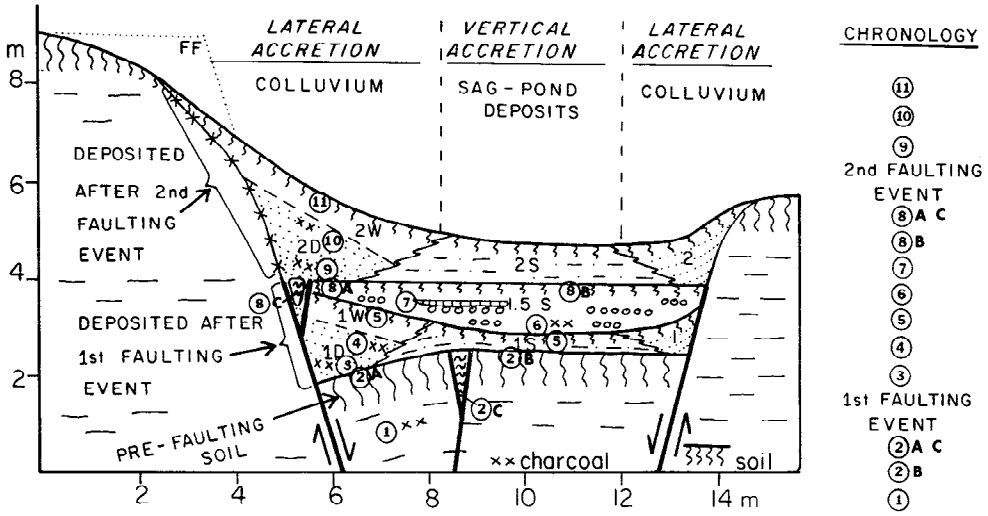

Figure 2. Schematic cross section through a normal fault scarp and graben formed by two surface-faulting events; this is a composite section showing features observed in many trenches across the WFZ. Colluvium shed from the main scarp (at left) is divided into debris facies (D) and wash facies (W); both facies grade into coeval sag pond deposits (1S, 2S). Between faulting events a fluvial deposit (1.5S), containing lenses of gravel (circles), completely filled the graben. Circled numbers indicate potential sites for obtaining radiocarbon samples, and the chronology at right shows which samples most closely constrain the times of the faulting events. Debris facies colluvium is deposited immediately after faulting, whereas sag pond deposition may be climatically controlled and postdate faulting by decades. Radiocarbon dates from sites 2A and 8A have traditionally been interpreted as the closest maximum limiting ages on faulting, as shown on the chronology at right. However, if radiocarbon ages from soils 2 and 8 are mean residence time corrected to reflect the age of soil burial, they become minimum age constraints on faulting, with the closest constraint closest to the fault. Most of the numerical ages in Table 1 are from positions 2A/8A or 2C/8C. Ages labeled "min" in Table 1 are from positions such as 3 and 9. Samples from wash facies colluvium (5, 11) and interbedded fluvial deposits (6, 7) do not provide close age constraints on faulting.

ages that most closely constrain the times of paleoearthquakes. Paleoearthquake studies on the WFZ can be divided into three time periods. Between 1977 and 1984, Woodward-Clyde Consultants identified and trenched each of the central fault segments [*Swan et al.*, 1980, 1981a, b; *Hanson and Schwartz*, 1982; *Schwartz et al.*, 1983; *Schwartz and Coppersmith*, 1984]. Most ^{14}C ages from these trenches were derived from charcoal, either detrital or in situ burns. Charcoal fragments have the advantage of containing carbon with a short age span (unlike soils) but the disadvantage of typically not lying near the event horizon. Buried soils and organic fissure fills nearer to the event horizons were mapped but were generally not dated (compare work by *Swan et al.* [1980] with work by *McCalpin et al.* [1994]), because workers at the time were uncertain how to interpret ^{14}C ages on soil organics of mixed origins and ages. Thus most of the ^{14}C ages from these early studies provided only approximate age constraints (albeit better than no constraints) on paleoearthquakes.

Between 1984 and 1989 the U.S. Geological Survey (USGS) performed intensive studies at multiple trench sites on the central segments [*Lund and Schwartz*, 1987; *Machette and Lund*, 1987; *Machette*, 1988a, b; *Nelson*, 1988; *Personius*, 1988, 1991; *Schwartz et al.*, 1988; *Forman et al.*, 1989, 1991; *Jackson*, 1991; *Lund et al.*, 1991; *Machette et al.*, 1987, 1991, 1992a, b]. As of 1988, 47 trenches and four natural exposures had been logged and sampled at 20 sites on six segments of the WFZ [*Machette et al.*, 1992a]. These studies included ^{14}C dating of charcoal and buried soils, the latter of which reflected increased confidence and experience in dating soil organics. Experimental thermoluminescence dating of several facies was also begun [*Forman et al.*, 1989, 1991; *McCalpin and Forman*, 1991]. All the numerical ages from the USGS trenches (but not from earlier Woodward-Clyde trenches) are inventoried by *Machette et al.* [1992a, Appendix], who list 55 ages (38 ^{14}C, 17 thermoluminescence).

From 1989 to present, additional trench studies have continued under USGS funding. These include 14 trenches across a zone of distributed fault scarps in the Brigham City segment [*McCalpin and Forman*, 1993], one trench on the Weber segment [*McCalpin et al.*, 1994], and eight trenches on the Salt Lake City segment [*Lund*, 1992; *Black and Lund*, 1995; *Black et al.*, 1995]. Data from these studies are either published only in abstracts [e.g., *Lund et al.*, 1990; *Ostenaa*, 1990] or are unpublished, so we obtained the original laboratory ages and trench logs from the authors (Table 1).

We next examined the logs of sampled trenches to identify those samples whose stratigraphic position most closely constrains the time of faulting. Our criteria are based on the stratigraphic concepts summarized in Figure 2. Three stratigraphic settings (event horizons buried by proximal colluvium and graben sediments, and basal fissure fills) provide the most closely limiting ages on paleoearthquakes, and all have traditionally been interpreted as maximum limiting ages. The closest limiting ages are almost always derived from buried A horizons beneath proximal debris-element colluvium within ~5 m of the fault (Figure 2, locations 2A and 8A). We chose this distance because the 35°-sloping apron of debris-element colluvium rapidly shed from a (typical) 2 to 4 m-high free face will extend roughly 3-5 m from the scarp after faulting [*Wallace*, 1980, 1984]. The next closest limiting ages come from filled fissures (Figure 2, locations 2C and

8C), which begin to fill with soil-derived organics soon after faulting [e.g., *Crone et al.*, 1987]. Buried soils in graben or back-tilted areas (Figure 2, locations 2B and 8B) provide the next closest limiting ages on faulting. However, it is often difficult to estimate the time that elapsed between faulting and renewed deposition in the graben, so it is possible that the soil in a graben could continue to develop for years or decades after faulting before it was buried.

Few closely limiting minimum ages on paleoearthquakes exist because detrital organics are rarely found in the debris-element colluvium overlying the event horizon. The most closely limiting minimum ages are typically found in wash-facies colluvium and sag pond deposits that overlie the event horizon, but these ages postdate the earthquake by the unknown amount of time needed to degrade the scarp to wash-dominated state or to fill the graben with its initial sediments. The 13 minimum ages felt to be most closely limiting are included in Table 1. However, only five of the 16 Holocene paleoearthquakes are constrained by these minimum ages, so they cannot be used in a systematic manner for bracketing earthquake ages or for calculating recurrence times.

Based on our stratigraphic model, we do not consider numerical ages derived from the following as closely limiting: (1) soils buried by colluvium >5 m from the fault, (2) soils buried by wash-element colluvium far from the scarp, (3) organics in fluvial sediments deposited against the scarp, and (4) any samples separated from the event horizon to be dated by an unconformity. Based on the above stratigraphic criteria, 89 (76 maximum limiting ages and 13 minimum limiting ages, or 32%) of the 276 existing numerical ages can be considered as closely limiting the dates of Holocene paleoearthquakes on the WFZ (Table 1).

Most event horizons exposed in WFZ trenches are the upper horizon contacts of buried soils. We follow the procedure of *Machette et al.* [1992a, Appendix] to estimate the age of the upper horizon contact from ^{14}C and therm-oluminescence ages derived from subjacent soil material. First, we calibrate the laboratory ^{14}C ages for secular variations in ^{14}C production, using the dendrochronologic-calibration program CALIB v. 3.0 [*Stuiver and Reimer*, 1993]. This calibration program requires input of the carbon age span in the sample. Limited data on the trend of increasing ^{14}C age with depth in weakly developed, buried soils in Utah and western Wyoming indicate that a typical 10-cm-thick sample carries a carbon age span of 200-400 years (Table 2). CALIB v. 3.0 only permits a maximum carbon age span input value of 300 years, which is used in cases where the sample carbon age span is inferred to be ≥300 years.

The calibrated age of the soil sample is then corrected for the mean residence time of carbon in the sample. This correction is necessary because the dated soil did not have an age of zero years when buried by scarp-derived colluvium but would have yielded (on the day of burial) an age representing the mean age of carbon that resided in the finite thickness of soil sampled. In essence, mean residence time correction as proposed by *Machette et al.* [1992a] and practiced herein is equivalent to extrapolating the age of the upper horizon contact from the age of the underlying 5-10 cm of soil, assuming that (1) the calibrated age represents the age of the center of the sampled interval, and (2) the trend of age with depth is approximately linear, as illustrated in Figures 3c and 3d. Table 2 shows values of mean residence time derived from both modern and buried soils on the Wasatch Front and in western Wyoming and the values suggest that a 10-cm-thick sample would carry an mean residence time of ~230 years. *Machette et al.* [1992a, Appendix] commonly assume an mean residence time of 200 years for the 5 to 10-cm-thick samples collected in their WFZ trenches. An independent method for estimating mean residence time in soils is to compare ^{14}C ages on bulk soil with ^{14}C ages on charcoal from the same soil. *Hanson and Schwartz* [1982] note that at the North Creek site on the Nephi segment, a bulk soil dated at 1650±50 ^{14}C years B.P. (conventional age) and 1645 +270/-262 ^{14}C years B.P. (accelerator mass spectrometry age), yielded a charcoal age of 1389 +181/-177 ^{14}C years B.P. The

Table 1. Numerical Ages That Constrain Paleoearthquakes on the WFZ

Trench[a]	Source[b]	Lab No.[c]	Material[d]	Geologic Unit[e]	Lab 14C age (14C yr B.P. or TL age[f] (cal yr B.P.)	CAS/ MRT (cal yr BP)[g]	MRT-Corrected Age of Event Horizon	Paleo-earthquake Constrained[h]
				Brigham City Segment				
T12	1	B-68254	A	PC	1720±90	a	1691(1412)1142	Z, min
T2	1	OTL-403	Av	L	1.7±0.2,2.1±0.3	-	1900±300Z	
T13	1	B-68256	Ab	CF	2320±70	a	2251(2020)1801	Z
T14	1	B-68258	Ab	PC	2580±60	a	2680(2513)2200	Z
T12	1	B-68253	Ab	PC	2630±90	a	2767(2571)2187	Z
T13	1	B-68255	Ab	PC	3320±80	a	3615(3344)3085	Y
BC-1	2	USGS-2535	Ab	PC	3430±70	b	3687(3462)3166	Y
T5	1	B-54890	Ab	PC	3430±60	a	3700(3476)3261	Y
PP-1	2	PITT-0093	A	CF	4190±125	c	4880(4579)4107	X
BC-1	2	USGS-2536	Ab	DF	4330±70	c	4929(4695)4505	X
BC-1	2	USGS-2604	Ab	DF	4340±100	c	5120(4700)4351	X
T14	1	B-68257	Ab	PC	5380±80	c	6213(5970)5730	W
T2	1	OTL-402	Av	L	7.3±0.7 ka	-	7300±700	V
T3	1	OTL-404	Av	L	8.3±1.3 ka	-	8300±1300	U
T6	1	OTL-421	Av	L	8.6±0.8 ka	-	8600±800	U
T6	1	B-54889	C	L	13,010±460	-	~13-13.5 ka[i]	T

Table 1. (continued)

Trench[a]	Source[b]	Lab No.[c]	Material[d]	Geologic Unit[e]	Lab 14C age (14C yr B.P. or TL age[f] (cal yr B.P.)	CAS/ MRT (cal yr BP)[g]	MRT-Corrected Age of Event Horizon	Paleo-earthquake Constrained[h]
					Weber Segment[j]			
K-88	1	B-29901	Ab	DC	900±80	b	917(683)550	Z
GC	2	NSRL-523	Ab	PC	990±80	b	978(821)587	Z
EO-2	3	PITT-0096	Ab	PC	1065±30	b	954(882)602	Z
K-88	1	B-29902	Ab	DC	1130±70	b	1140(920)784	Z
EO-2	3	PITT-0098	Ab	PC	1365±40	d	1228(1098)943	Z
EO-1	3	ITL-47	A	DC	1200±200	-	1200±200	Z
K-88	1	B-38680	A	CF	2220±50	e	3145(2821)2465	Y, min
GC	2	NSRL-520	Ab	PC	2490±100	f	2725(2588,2521, 2413)2224	Y
EO-2	3	ITL-74	Ab	PC	3200±300	-	3200±300	Y
EO-2	3	PITT-104	Ab	PC	3295±130	g	3818(3450)3165	Y
EO-2	3	ITL-80	Ab	L	4000±400	-	4000±400	X
EO-2	3	USGS-2499	C	DF	4100±180	-	5045(4564)4087	X
EO-2	3	PITT-0094	Ab	DF	4505±65	a	5032(4755)4471	X
EO-1	3	ITL-138	L	DF	4600±400	-	4600±400	X
K-88	1	ITL-150,171	Ab	DC	5850±636	-	5850±636	W
K-88	1	ITL-150,171	Ab	DC	6100±404	-	6100±404	W
K-88	1	B-29900	Ab	DC	5780±90	a	6651(6389)6116	W
					Salt Lake City Segment[k]			
DC-2	3	B-21303	Ab	PC	1170±60	c[l]	1103(862)700	Z
DC-1	1	B-54646	Ab	PC	930±60	b	912(741)579	Z
DC2-2	2	B-77139	OM	CF	1570±60	h	1393(1146)927	Z
DC2-3	2	B-77141	Ab	PC	1420±60	b	1349(1227)1103	Z
DC2-4	2	B-79188	OM	CF	1620±60	h	1446(1193)958	Z
DC2-1	2	B-80845	Ab	PC	1850±60	i	1797(1632)1415	Z
DC-2	1	B-28320	Ab	PC	1640±50	c[l]	1508(1318)1136	Z
DC-1	3	B-21304	Ab	PC	1830±80	c	1785(1564)1279	Z
DG-1	1	B-50879	Ab	PC	1760±60	b	1738(1559)1381	Z
DG-1	1	B-50880	Ab	PC	2370±70	b	2600(2277)2103	Y
DG-1	1	B-54017	Ab	PC	2410±60	b	2621(2303)2164	Y
DC2-5	2	B-79184	Ab	PC	2940±60	i	3177(2932)2691	Y
DC2-4	2	B-79920	OM	CF	3760±80	h	4172(3794)3480	X
DC2-2	2	B-77140	Ab	PC	3810±90	j	4304(4035)3748	X
DC-1	1	B-54649	Ab	PC	4520±60	b	5300(5114)4812	W
DC-1	3	B-21300	Ab	PC	4910±100	c[l]	5745(5452)5140	W
DC-2	3	B-21302	Ab	PC	4710±90	c	5516(5214)4958	W
DC-1	3	B-21299	Ab	PC	5230±80	c[l]	6074(5790)5545	W
					Provo Segment[m]			
Map.N1	1	PITT-0191	C	DF	330±50	-	502(425,392,319) 287	Z, min
AmFk.2	2	ITL-3	S	SP	500±200	-	500±200	Z, min
Map.N1	1	B-21306	C	L	445±70	-	551(505)311	Z, min
Map.N1	1	PITT-0188	C	L	490±65	-	635(517)334	Z, min
RockCr.	2	PITT-0091	Ab	DF	455±35	k	666(606)549	Z, min
RockCr.	3	-	Ab	DF	-	l	590±90	Z, min
WC 1	4	B-23781	C	PC	320±120	-	542(403)0	Z
AmFk.1	2	ITL-23	Ab	PC	400±100	-	400±100	Z
AmFk.2	2	USGS-2533	Ab	PC	620±150	k	760(494)221	Z
Map.N1	1	PITT-0189	C	PC	730±40	-	715(664)576	Z
AmFk.1	2	USGS-2532	Ab	PC	980±70	a	905(696)468	Z
Map.N2	1	B-21733	C	PC	770±100	-	919(672)547	Z
WC 1	4	B-23779	C	DF	890±60	-	931(782)671	Z
WC 1	4	B-23778	C	DF	950±60	-	961(909,800)724	Z
RockCr.	2	DIC-3236	A	PC	1110±50	c	985(806)670	Z
RockCr.	3	-	Ab	DF	-	m	810±130	Z
AmFk.1	2	USGS-2531	Ab	PC	2620±70	a	2723(2545)2293	Y
AmFk.1	2	ITL-16	Ab	PC	2700±200	-	2700±200	Y
Map.S1	1	B-26117	Ab	PC	2890±80	d	3128(2807)2550	Y

Table 1. (continued)

Trench[a]	Source[b]	Lab No.[c]	Material[d]	Geologic Unit[e]	Lab 14C age (14C yr B.P. or TL age[f] (cal yr B.P.)	CAS/ MRT (cal yr BP)[g]	MRT-Corrected Age of Event Horizon	Paleo-earthquake Constrained[h]
					Provo Segment[m]			
Map.S1	1	B-23527	C	PC	2810±95	-	3207(2876)2751	Y
Map.S1	1	ITL-70	Ab	PC	330±300	-	3300±300	Y
AmFk.	2	AA-2266	C	DF	4740±90	-	5649(5562,5549, (5468)5262	X
WC 2	4	B-24178	C	DF	4600±75	-	5567(5306)4996	X
					Nephi Segment[n]			
NCr.1	1	Wc-12-80-4	C	DC	263,+219/-213	-	660(298)0	Z, min
NCr.3	1	WC-12-80-10	C	DC	502,+607/-566	-	1685(522)0	Z, min
WC 2	4	B-24815	C	PC	710±90	-	782(660)534	Z, min
NCr.3	1	WC-12-80-6	C	PC	922,+151/-148	-	1162(888,873,825, 816)792	Z
NCr.2	1	WC-12-80-5	Ab	PC	1350±70	a	1262(1086)828	Z
NCr.3	1	WC-12-80-6	C	PC	1110±60	-	1165(983)924	Z
WC 1	4	B-24818	Ab	PC	1530±60	a	1408(1210)1065	Z
RedCyn	3	ITL-88	Ab	PC	1300±500	-	1300±500	Z
RedCyn	3	ITL-67	Ab	PC	1500±400	-	1500±400	Z
WC 2	4	B-24814	Ab	PC	1850±70	a	1776(1561)1324	Z
WC 2	4	B-24180	C	PC	3445±100	-	3966(3690)3464	Y, min
WC 2	4	B-24808	C	PC	3655±120	-	4349(3971,3949, 3932)3637	Y
NCr.3	1	WC-12-80-7	Ab	PC	3640±75	a	4427(4144)3874	Y, min
RedCyn	3	B-25185	A	CF	3550±150	a	4122(3624)3192	Y
RedCyn	3	B-25184	Ab	PC	3690±170	b	4423(3900)3429	Y
NCr.3	1	WC-12-80-7	Ab	PC	3894,+288/-278	n	5079(4147,4125, 4103)3287	Y

[a] T,Provo delta east of Brigham City; BC, Brigham City; K88, Kaysville 1988 trench; GC, Garner Canyon exposure; EO, East Ogden; DC-1, DC-2, Dry Creek; DC2-1 through 2-5, South Fork Dry Creek; DG, Dry Gulch; Map.N, Mapleton North; Map.S, Mapleton South; AmFk., American Fork; RockCr, Rock Creek at Provo, Utah; WC, Water Canyon; NCr., North Creek; WC, Water Canyon; RedCyn, Red Canyon. Numbers indicate the local trench numbering scheme.

[b] Sources: 1, J.P. McCalpin and S.L. Forman, unpublished data, 1994; 2, *Personius* [1991].

[c] B, Beta Analytic, Inc.; USGS, U.S. Geological Survey radiocarbon laboratory, Menlo Park, California; PITT, University of Pittsburgh radiocarbon laboratory; NSRL, National Science Foundation radioisotope laboratory, Tucson, Arizona; AA, also NSF lab. but accelerator mass spectrometry date; DIC, Dicarb Radioisotope Co.; WC, field identifier from Woodward-Clyde Consultants; OTL, Luminescence dating laboratory, Ohio State University; ITL, Luminescence dating laboratory, Institute of Arctice and Alpine Research, Boulder, Colorado.

[d] A, organic A horizon; Av, vesicular (non-organic) A horizon; Ab, buried horizon); C, charcoal; S, inorganic silt.

[e] PC, proximal (debris-facies) colluvium; DC, distal (wash-facies) colluvium; CF, tectonic crack fill; DF, debris flow; SP, sag pond sand and silt; L, loess.

[f] CAS, carbon age span within sample (inferred; see *Machette et al.* [1992a, Appendix]. Taken from published source of from collector's recommendation. MRT= mean residence time (see Machette et al., 1992a, Appendix). Taken from published source or from collector's recommendation. The uncertainty was added by us; see text for derivation. Letter codes represent the following CAS/MRT combinations (in years): a, 300/200±75; b, 200/100±38; c, 200/200±75; d, 250/200±75; e, 300/600±225; f, 100/100±38; g, 100/50±19; h, 200/300±112; i, 200/150±56; j, 100/150±56; k, 150/100±38; l, 250/0; m, 450/0; n, 0/200±75. Uncertainties are derived from the age trend with depth relation described in Table 2.

[g] Calculated by computing the dendro-corrected age, using the computer program CALIB 3.0 of *Stuiver and Reimer* [1993], with: 10-year atmospheric calibration data set, carbon time span, CAS, laboratory error multiplier, 1. For UHC, final age is dendro-corrected age minus MRT; for LHC, final age is dendro-corrected age plus MRT. Ages flanking mean age (in parentheses) are 2σ limits, as defined by the CALIB program. Age range is 2σ and includes analytical and sample context uncertainties.

[h] Events are lettered from latest (Z) to earliest (W). All ages are considered very close minimum age limits on paleoearthquake age, except for those minimum ages (min.) from thermoluminescence or charcoal that lay stratigraphically above the event horizon and could not be extrapolated to the UHC or LHC.

[i] this subaerial soil was exposed after the abandonment of the Provo shoreline, dated at ~13-13.5 ka.

[j] Sources: 1, *McCalpin et al.* [1994]; 2, *Stafford and Forman* [1993]; 3, *Machette et al.* [1992a].

[k] Sources: 1, W.R. Lund, unpublished data, 1994; 2, *Black and Lund* [1995]; *Black et al.* [1995]; 3, *Schwartz* [1988b].

[l] Minimum values for 20 to 30-cm-thick channel samples.

[m] Sources: 1, *Lund et al.* [1991]; 2, *Machette et al.* [1992a]; 3, *Lund et al.* [1990]; 4, D.A. Ostenaa, unpublished data, 1994.

[n] Sources: 1, *Hanson and Schwartz* [1982]; 2, D.A. Ostenaa, unpublished data, 1994; 3, *Jackson* [1991].

Table 2. Data Used to Estimate Mean Residence Times and Carbon Age Spans for Soils

Reference	Data	Age Trend yr/mm	Number of Ages[a]
Machette et al. [1992a, p. A70	"upper 3-20 cm of a modern 10-40 cm-thick A horizon would yield AMRT ages of 100-400 years, if no bomb carbon was present"	4.0-6.67	nd
Forman et al. [1991]	age trend in distal colluvium affected by cumulic soil development ranges from 1 to 10 cm/100 years	1-10	1 series of 3; 1 series of 7
Stafford and Forman [1993]	age trend in upper 10 cm of soil= 0.27 mm/yr, increasing to 0.8-2.1 mm/yr at depths of 15-25 cm and 5.0 mm/yr below 25 cm	3.7 (in upper 10 cm); 0.2-0.5 (below 15 cm)	2 series of 3; 1 series of 6
J.P. McCalpin (unpublished data, 1994, from Rock Creek fault, Wyoming)	in a 40 cm-thick horizon, roughly linear age trend of 0.3 mm/yr between 2260 and 3280 ^{14}C year BP (Figure 3)	4.1	1 series of 4
Mean age trend in debris facies soils[b]		4.6 (range 3.7-6.7)	

[a] Described as the number of series (vertical transects) followed by the number of samples within each series

[b] For a 10-cm-thick sample, the difference between the age of the center of the sample and the top of the sample (upper horizon contact) can be calculated as the product of age trend times 50 mm, yielding a range of 185-335 years (mean 230 years). We assume that the 150-year spread between age estimates roughly represents $\pm 2\sigma$ uncertainty associated with mean residence time correction.

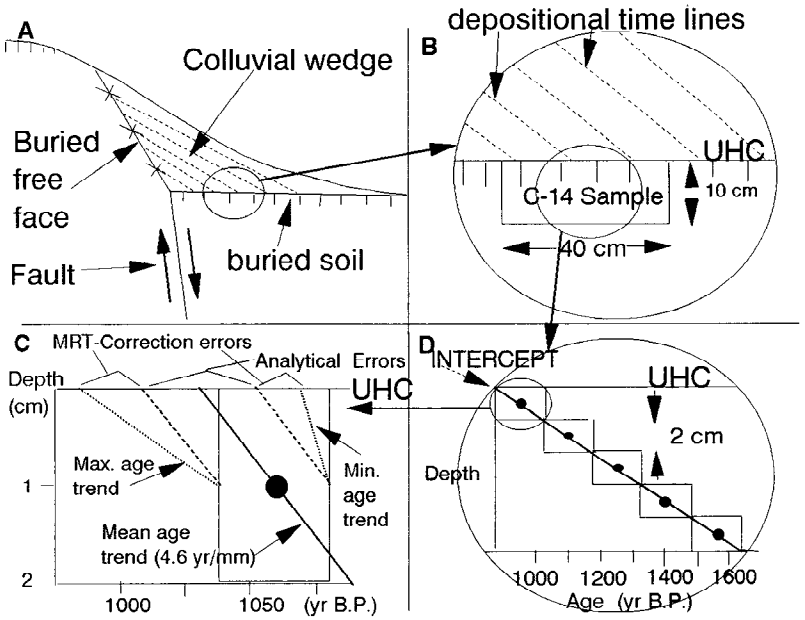

Figure 3. Idealized diagrams of a single-event normal fault scarp showing various sources of uncertainty in relating numerical ages to the time of paleoearthquakes. (a) simplified cross-section of the colluvial wedge. Dashed lines show depositional time lines in colluvium. (b) close-up view of a typical radiocarbon sample, emphasizing the time-transgressive nature of the event horizon (i.e., burial of the upper horizon contact of the soil). (d) close-up of the 10 cm-thick radiocarbon sample, showing the trend of increasing age with depth (compare to Figure 4) and the principle of extrapolating the age of the upper horizon contact. (c) close-up of how age uncertainties are calculated for the event horizon (upper horizon contact) immediately above the dated sample. Cross shows mean radiocarbon ages with 2σ limits; solid square shows dendro-corrected radiocarbon age, with 2σ limits shown by the horizontal dimension of the surrounding box. Vertical dimension of the box indicates sample thickness. Solid line shows a least-squares regression lines through the dendro-corrected mean ages. The top of the graph represents the upper horizon contact of the soil. The total 2σ error range on age of the upper horizon contact is composed of an analytical component and a sample context component. The analytical component is defined by extrapolations of the mean age trend (4.6 yr/mm) from the $\pm 2\sigma$ limits on the age of the uppermost 10 cm-thick sample (dashed lines). The sample context component is defined by extrapolations of the maximum age trend (6.7 yr/mm) from the -2σ age limit and the minimum age trend (3.7 yr/mm) from the $+2\sigma$ age limit (dotted lines).

mean bulk soil ages were thus 256-261 years older than the mean charcoal age, although the age estimates overlap at 2σ.

The additional error introduced by mean residence time correction comprises part of the overall sample context error [Taylor, 1987] in relating the numerical age to the time of the paleoearthquake (the remainder of sample context error is the time required for colluvium to advance and bury the soil). The mean residence time correction error varies with the thickness and carbon content of each sample and is thus difficult to estimate precisely. A rough approximation of the error (Figure 3d) can be estimated by extrapolating the minimum (3.7 yr/mm) and maximum (6.7 yr/mm) age trends (Table 2) over a 5-cm distance (typical sample half-thickness) from a common age point; this amounts to a 150-year spread, or ±75 years. We assume that this age spread between the minimum and maximum intercepts captures almost all of the age uncertainty and approximates the ±2σ limits on age; however, more studies on age/depth relations would be necessary to strictly validate this assumption. Following *Machette et al.* [1992a], we thus use 200 years as a default value for mean residence time, with an estimated 2σ uncertainty of ±75 years. If trench loggers indicate that samples were abnormally thinner (e.g., samples at Dry Creek, Salt Lake City segment [*Lund*, 1992] that ranged from 2 to 5 cm thick) we decrease the mean residence time and its uncertainty proportionally.

For charcoal samples the mean residence time and carbon age span are considered to be negligibly small, so the calibrated age is not further corrected (Table 1). However, since charcoal samples lie at some distance above or below the upper horizon contact and have not been adjusted (extrapolated) for the intervening stratigraphic distance (we do not know sedimentation rates for all fault zone facies), they are considered to be less closely limiting ages than are soil-derived dates.

The 89 closely limiting ages in Table 1 include 15 thermoluminescence age estimates. To use these thermoluminescence age estimates in a combined analysis with ^{14}C ages, we must contend that there is no systematic offset between the calibrated ^{14}C time scale and the thermoluminescence time scale. Previous work on the WFZ demonstrated the concordance of thermoluminescence age estimates with ^{14}C ages from the upper parts of soil A horizons [*Forman et al.*, 1989, 1991]. This same concordance has been observed elsewhere by *Huntley et al.* [1983], *Wintle and Catt* [1985] and *Berger* [1988] and is attributed to effective sunlight bleaching of silt grains exposed by bioturbation, which resets the thermoluminescence clock to zero.

Ages derived from buried soils beneath event horizons are often interpreted as maximum limiting ages for paleoearthquakes. This interpretation is understandable, since the dated soil lies stratigraphically beneath the event horizon and much of the dated soil carbon accumulated before faulting. However, when we correct soil age for mean residence time, we are estimating the time when the upper horizon contact of the soil was buried by postfaulting sediments, and this time is of course younger than the time of the paleoearthquake. For locations >5 m from the fault, the soil may not be buried by scarp-derived colluvium for decades or centuries after faulting, and thus the mean residence time-corrected age of the soil upper horizon contact >5 m from the fault constitutes a loosely constrained minimum age limit on faulting, even though the dated material actually came from beneath the event horizon. The difference between the time of the earthquake (scarp formation) and the time that the soil upper horizon contact is buried by colluvium close to the fault is (by analogy to historic fault scarps) only a few years to decades [e.g., *Wallace*, 1977, 1980, 1984]. This time span is considerably less than the 2σ analytical uncertainties associated with dendro-corrected ^{14}C ages (100-300 years) and suggests that for all practical purposes, the 89 mean residence time-corrected limiting ages in Table 1 can be considered as dating the paleoearthquakes themselves. Due to the large age uncertainties, we round off age estimates and 2σ age limits cited in the text to the nearest decade.

Holocene Earthquakes on the WFZ in Space and Time

The space-time diagram in Figure 4 summarizes the mid- to late Holocene earthquake history for the five central segments of the WFZ, based on the 89 limiting ages in Table 1. Numerical ages come from trenching studies through the summer of 1994, and they indicate 16 paleoearthquakes since ~5.6 ka. A major difference from earlier space-time diagrams is the addition of three "new" paleoearthquakes, event Z on the Brigham City segment [*McCalpin and Forman*, 1993] and events X and Y on the Salt Lake City segment [*Black et al.*, 1995], and the deletion of a very recent event (~500 years B.P.) on the Weber segment [see *McCalpin et al.*, 1994]. Four of the five segments have experienced three paleoearthquakes in that time span, whereas the Salt Lake City segment has experienced four large earthquakes. The boxes in Figure 4 illustrate how tightly the maximum limiting ages cluster for any given earthquake. Our portrayal of earthquake timing differs from that of *Machette et al.* [1992a, b] and earlier workers by plotting the limiting ages directly, instead of bracketing earthquake ages with minimum and maximum permissible limits.

We compute the weighted mean age (T) in cal yrs for each paleoearthquake by using the arithmetic mean of the 2σ analytical uncertainty in Table 1 as a weighting factor,

$$\overline{T} = \frac{\sum_{i=1}^{n} t_i \left(\frac{1}{\sqrt{\sigma_i^2}}\right)}{\sum_{i=1}^{n} \frac{1}{\sqrt{\sigma_i^2}}} \quad (1)$$

where t_i is the individual age determination and its associated error σ_i. The standard deviation of the weighted mean age is

$$\overline{\sigma} = \sqrt{\frac{1}{\sum_{i=1}^{n} \left(\frac{1}{\sigma_i^2}\right)}} \quad (2)$$

(Equations (1) and (2) are from *Geyh and Schleicher* [1990]).

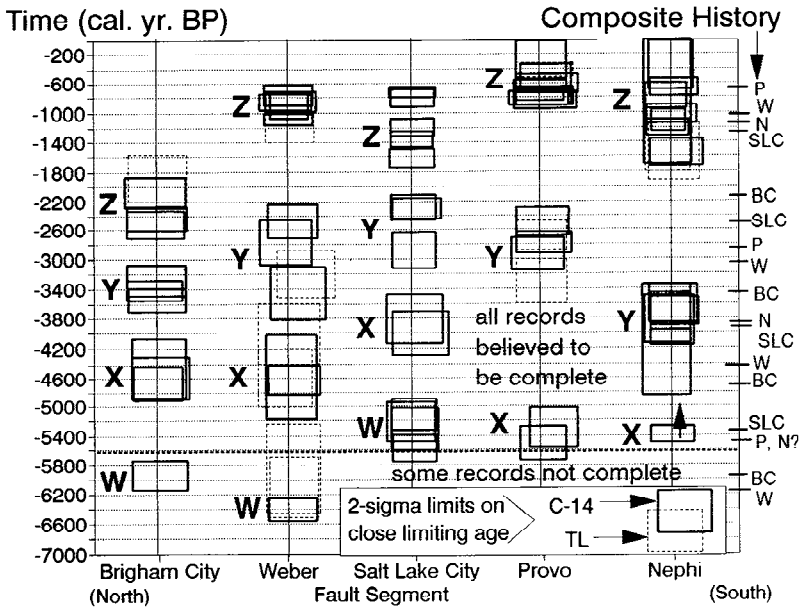

Figure 4. Space-time diagram of earthquakes in the past 7000 years on the central five segments of the WFZ; earthquake histories younger than 5600 cal years B.P. (dashed line) are believed to be complete. For each segment, individual paleoearthquakes are labeled from Z (youngest) to W (oldest). Each of the 76 maximum limiting age estimates listed in Table 1 is plotted as a box (solid for ^{14}C, dashed for thermoluminescence). The height of each box equals the $\pm 2\sigma$ uncertainties (analytical plus sample context) in calendar age. On the Nephi segment, a paleoearthquake was inferred by *Hanson and Schwartz* [1982] between event Y and 5220-5475 cal years B.P., but age control was so indirect that the event is only represented by a maximum age arrow. Weighted mean ages for all earthquakes on all segments are merged onto a composite paleoseismic history at the right side of the figure.

Calculation of weighted means for each lettered earthquake on Figure 4 assumes that earthquakes dated by groups of close ages (often from different trenches) within a segment are in fact the same earthquake. This assumption can be tested by computing the chi-square statistic for all numerical ages within a group, and testing for significance at the 1% level. Using this test, 11 of our 76 limiting ages do not belong to their respective groups. However, we do not discard those ages from our analysis because we regard the variation in soil ages in a given group as the result of stochastic processes operating on the scale of centimeters and decimeters (burrowing, carbon remobilization) that are impossible to isolate in detail at this time. We note there is no clear relation among sampled trenches on the WFZ between ages of buried soils and distance from the fault (a proxy for the time required to bury the soil after faulting). This lack of correspondence among trenches suggests that colluvial wedges prograde at different rates in different locations. In some trenches (e.g., Dry Creek [*Lund*, 1992] replicate soil samples from the same position in a trench have yielded varying ages. If all buried soils in a segment carried exactly the same radiocarbon age at time of burial after a given paleoearthquake, and later burrowing could be discounted, then variation in limiting ages for a given earthquake could only be explained by analytical uncertainties and the time-transgressive nature of the event horizon. If this were true, then only the youngest maximum limiting age should be used to constrain the age of each paleoearthquake, and the other maximum ages should be construed as less closely limiting. However, on the WFZ we suggest that the variation of limiting ages for a given paleoearthquake is due to unpredictable variations in soil radiocarbon age at the time of burial or to later burrowing and to variable rates of colluvial progradation among trench sites, not to the predictable time-transgressive nature of the event horizon. Because we cannot prefer any of the 76 close limiting ages over others on purely stratigraphic grounds, we do not discard those 11 ages with anomalously high chi-square values.

The weighted mean ages for each paleoearthquake (Table 3) have been transferred onto a single time line on the right side of Figure 4, to show the composite paleoseismic history for the central WFZ. This composite history contains 16 earthquakes (post-5.6 ka) with mean interevent time of 347 years, standard deviation of 228 years, and coefficient of variation of 0.66. For the qualitative tests and comparisons that follow, we only examine that part of the space-time diagram where we are confident (based on multiple trenching studies) that all large surface-rupturing earthquakes have been identified. While the record of dated paleoearthquakes for some segments extends back to 13 ka (Brigham City segment [*McCalpin and Forman*, 1993], the shortest record among the five segments dictates the useful length of the composite record. At most trench sites, the oldest geomorphic surface trenched was a mid-Holocene (5-6 ka) alluvial fan [*Machette et al.*, 1992a]. Thus our analysis of the composite record extends only back to a common time limit of ~5.6 ka and excludes the two earliest dated paleoearthquakes on the Brigham City and Weber segments that were identified in excavations in late Pleistocene deposits.

Does the past 5.6 kyr of data (Figure 4) provide an adequate baseline for understanding large-earthquake recurrence along the WFZ? The following sections address

Table 3. Limiting Numerical Ages, Weighted Mean Age Estimates, and Recurrence Intervals for Paleoearthquakes on Central Wasatch Fault Zone

Segment	Event	Limiting Ages,[a] cal years B. P.		Weighted Interevent Time,[c] Mean ±2σ, cal years
		No.	Mean[b]±2 σ	
Brigham City	Z	4	2125±104	1309±176
	Y	3	3434±142	1240±220
	X	3	4674±108	1296±294
	W[d]	1	5970±242	1330±426
	V[d]	1	7300±350	1218±488
	U[d]	2	8518±340	4492±412
	T[d]	1	13,010	mean[e]= 1282±138
Weber	Z	6	1016±62	2048±130
	Y	3	3064±114	1339±108
	X	4	4403±122	1729±188
	W[d]	3	6132±144	mean[e]=1782±102
Salt Lake City	Z	9	1230±62	1269±152
	Y	3	2499±138	1442±258
	X	2	3940±216	1440±256
	W	4	5381±136	mean[e]=1441±182
Provo	Z	10	618±30[f]	2224±78
	Y	5	2842±72	2639±168
	X	2	5481±152	mean[e]=2297±70
Nephi	Z	7	1148±68	2716±248
	Y	5	3864±238	Mean[e]=2716±248
Totals		76	mean[e]=1918 years	

[a] Number of close limiting ages from Table 1; does not include less closely limiting minimum ages marked as "min" inTable 1.
[b] Mean weighted by the standard deviation.
[c] Interevent times and their uncertainties are computed by the weighting procedure to the nearest year but should be rounded off to the nearest decade for any derivative calculations.
[d] These earthquakes predate 5.6 ka and are not used in the synthetic modeling.
[e] Weighted mean±2σ over the past 5600 years, the period in which the paleoseismic record is considered complete for all five segments; see Equations (1) and (2).
[f] A bimodal distribution with modes at 495 years and 802 cal years B.P.
[g] Standard error of mean= 48 years (2σ); unweighted group mean= 1767 years, sample standard deviation= 585 years (1σ); coefficient of variation= 0.33.

two facets of this question: (1) the degree of temporal clustering of large earthquakes, and (2) the probability of a future large earthquake along the WFZ.

Tests for Temporal Clustering and Earthquake Contagion

The four most recent earthquakes along the central WFZ occurred within the past 1.2 kyr, when four out of five segments ruptured between (mean ages) 620±30 and 1230±60 cal years B.P. (permissible 2σ time range 520-700 cal years B.P.). *Machette et al.* [1992a, p. A50] interpreted these data to indicate that earthquakes on the WFZ have a tendency to occur in clusters. Prior to the most recent earthquake cluster, however, the space-time distribution of earthquakes along the central WFZ in Figure 3 appears more random, as noted by *Schwartz* [1988a] and *Machette et al.* [1991, 1992a, b]. The nonpersistence of clustered behavior throughout the Holocene may reflect the degree of coupling between adjacent segments on the fault [*Cornell et al.*, 1993]. Loosely coupled fault systems exhibit less clustered behavior than more strongly coupled systems. The null hypothesis is that the pattern in Figure 4 is just the chance product of earthquakes occurring on completely independent segments.

Distinguishing between a causal versus a chance origin for temporal clusters is a critical need in paleoseismology and seismic hazard assessment. At present, probabilities of future earthquakes on fault segments are computed solely from the recurrence history and elapsed time of each individual segment [e.g., *Working Group on California Earthquake Probabilities* (WGCEP) 1988, 1990] and ignore the influence of regional clustering. If the effects of mechanical coupling between segments must also be considered, then any estimate of the likelihood of a future earthquake must take into account stress states and elapsed times of adjacent segments as well [e.g., *Cornell et al.*, 1993]. Inter-segment triggering of earthquakes has been termed "contagion" by *Perkins* [1987]. Below we outline a statistical method of testing observed paleoseismic histories against synthetically generated paleoseismic histories that were created without contagion. (Using standard statistical tests to compare the frequency distribution of recurrence in observed versus synthetic histories would not sufficiently characterize the spatial arrangement of clusters and gaps on a time line.) Synthetic earthquake histories have been used to model fault interactions along plate boundaries [see *Lay and Kanamori*, 1981; *Ward*, 1991, 1992, 1993], but have not been applied to test the strength of clustering or fault interaction using paleoseismic histories of multisegment faults in intraplate environments.

The terms temporal cluster and gap, as applied to characteristic earthquakes, have not been well-defined in previous literature. For example, temporal cluster has commonly been used to describe large earthquakes that are anomalously close in time on a single fault or fault segment, but the term can also be used to describe closely timed large earthquakes occurring on different segments of a fault (such as in the WFZ space-time diagram), or on different faults in a fault system (such as the post-1872 temporal cluster of earthquakes in the California-central Nevada Seismic Belt [*Wallace*, 1987]). Definitions proposed in Table 4, which apply to any type of fault, will be used throughout the remaining discussion (e.g. Figure 5). An alternative to the clustering of large earthquakes on adjacent fault segments is multisegment ruptures. While this possibility is not explicitly treated in these simulations, we address this issue in a later section.

Generating Individual Synthetic Paleoseismic Histories

Individual synthetic paleoseismic histories are generated by assuming that the recurrence intervals between successive surface rupturing earthquakes obey some type of renewal model. Previous workers have theorized that recurrence

Table 4. Definition of Terms Used in Modeling Paleoseismic Histories

Term	Definition
Individual paleoseismic history	a chronological sequence of paleoearthquakes on a single fault or fault segment; earthquakes are represented as occurrences (points or boxes) or as probability distributions on a time line
Composite paleoseismic history	a chronological and spatial sequence of paleoearthquakes on several faults or fault segments; earthquakes are represented as occurrences (points or boxes) or as probability distributions on time lines; a composite history may be represented as several parallel time lines with a common scale and starting point (e.g., a space-time diagram such as Figure 5), or as a single time line onto which all earthquakes have been merged (right side of Figure 5)
Observed paleoseismic history	an individual or composite paleoseismic history reconstructed from field evidence and geochronology
Synthetic paleoseismic history	an artificially generated history of earthquakes, created either by direct generation of earthquake dates or by indirect generation of recurrence intervals according to some statistical distribution, and then stepwise summation of the recurrence intervals to form a chronological sequence
Cluster	a subjectively defined group of earthquakes, in any type of paleoseismic history (individual or composite, observed or synthetic), that occurs in a time span considerably shorter than the mean recurrence interval
Gap	a subjectively defined time gap between successive earthquakes, in any type of paleoseismic history (individual or composite, observed or synthetic), that seems anomalously long in comparison to the mean recurrence interval; often found flanking clusters

Any paleoseismic history must be either individual or composite, and observed or synthetic; e.g., the "space-time diagram" of the WFZ is an observed composite paleoseismic history; the synthetic histories for each fault segment used in the modeling are synthetic individual paleoseismic histories.

intervals may follow a normal [*Sykes and Nishenko*, 1984; *Bakun and Lindh*, 1985], lognormal [*Nishenko and Buland*, 1987], or Weibull distribution [*Nishenko*, 1985; *Sieh et al.*, 1989]. *Nishenko and Buland* [1987] conclude that the lognormal distribution best fits historic great earthquakes on subduction zones.

In this study we generate synthetic paleoseismic histories for the five central segments of the WFZ following 12 models; each model assumes a unique combination of frequency distribution, mean, and coefficient of variation (COV) for recurrence intervals (Table 5). For an aggregate of seismic sources, the sum of several non-Poisson processes has been demonstrated to approach a Poisson process [*Brillinger*, 1982; *Perkins*, 1987]. The Poisson models (1 and 2) were generated to develop a baseline for comparison with other distributions and to observe the effect of these models on the structure of the composite paleoseismic history. We consider it unlikely, however, that characteristic earthquakes occur as a Poisson process on individual fault segments. Characteristic earthquakes are thought to release virtually all the accumulated strain on a fault segment and thus restart the earthquake cycle [*Wu et al.*, 1995]. Models 3-6 assume that recurrence intervals on each segment follow a Gaussian distribution, despite the fact that its domain ($-\infty<T<\infty$) includes negative recurrence intervals [*Nishenko and Buland*, 1987, p. 1387]. In practice, however, Gaussian distributions centered around 2 ka with low coefficients of variation generate few negative values. Models 3 and 4 assume that the long-term mean recurrence interval of each segment is different and is equal to the weighted mean recurrence observed in the past 5.6 kyr (Table 3, column 5), whereas models 5 and 6 assume that the long-term recurrence is the same for all segments (set to 2000 years as an approximation of the composite mean recurrence of all segments; Table 3). Two coefficients of variation were modeled (0.3 and 0.5) to see what effect more variable recurrence on the individual segments would have on the composite paleoseismic history. Larger coefficients of variation for unimodal distributions were not specifically tested, however the Poisson models define a case where coefficient of variation is 1. Models 7-10 assume a lognormal distribution of segment recurrence intervals, using four variations similar to those used for the Gaussian models. The standard deviations of ln T/T_{avg} were set to 0.2 (after *Nishenko and Buland* [1987]) and 0.5 (bracketing the observed coefficient of variation of 0.33 from the WFZ segments; Figure 4). Models 11 and 12 assume Weibull behavior with the Weibull shape parameters (β) set to 3.5 and 2.0, respectively.

Generating Composite Synthetic Paleoseismic Histories

In each of the 12 models, the composite synthetic paleoseismic history was created by transferring the synthetic paleoseismic histories for all five individual segments (each segment containing 200 synthetic earthquakes) to a single time line (Figure 5). The composite histories are truncated at the end of the shortest of the five individual histories; otherwise, the composite history beyond that point would not include earthquake contributions from all segments. The synthetic composite histories created by models 1-12 thus span about 350-400 kyr, and each contains between 805 and 1060 earthquakes. The mean interevent time in composite histories ranges from 354 to 483 years. Coefficients of variation of interevent times are 1.03 for both Poisson-based models (models 1 and 2 in Table 5), indicating that the composite histories also approximate an exponential distribution. The

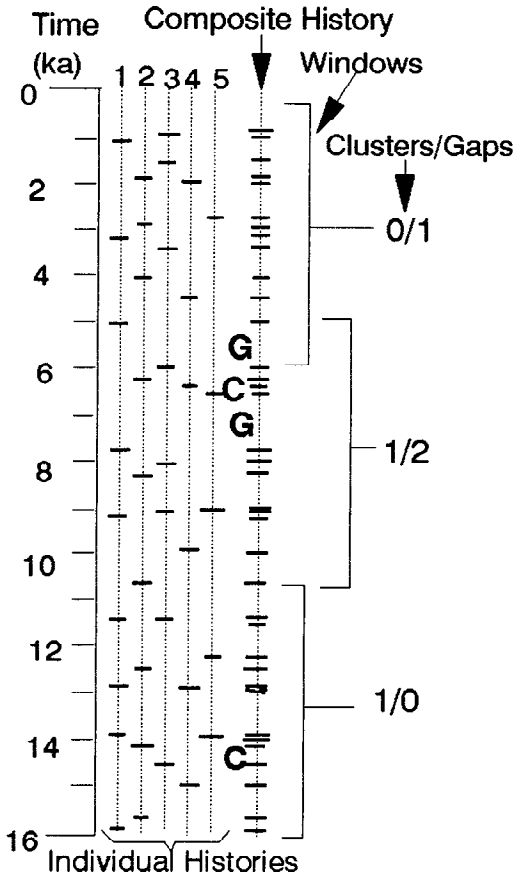

Figure 5. Example of synthetic paleoseismic histories. Earthquakes are shown as short thick lines on individual synthetic histories of each segment (dotted vertical lines); solid horizontal lines show how each event is collapsed onto the composite history (dashed line). Abbreviations are same as in text. This example shows the first 16 kyr of the 380 kyr record of model 4. Two 5.6-kyr window positions are shown, the upper one containing no clusters and one gap (as defined in text), the lower containing one cluster and no gaps.

other 10 models (with the exception of model 6) have coefficients of variation from 0.78 to 0.84, indicating a slightly more regular (less clustered) recurrence than the exponential distribution.

The Moving Window Test

The moving window test compares the pattern of observed earthquakes to patterns in randomly chosen time windows of the same length in synthetic composite paleoseismic histories [*McCalpin*, 1993]. Because the synthetic composite histories were created by adding five independently created individual histories (Figure 5), the synthetic composite histories contain no contagion effects and show only pseudo-patterns created by the actions of independent fault segments. As such, the synthetic composite histories form a "random baseline case" or null hypothesis against which to compare observed histories. We can thus ask, How often does the pattern of clusters and gaps in the observed composite paleoseismic history occur in a synthetic composite history that we know was generated randomly?. If the observed pattern occurs frequently in the synthetic record, we may conclude that a contagion mechanism is not necessary to explain the record, and thus we cannot rule out the null hypothesis. However, if the pattern of clusters and gaps in the observed record rarely (or never) appears in the synthetic histories, regardless of the type of recurrence models assumed for individual segments, we may conclude that the observed clustering is so unusual that it must be the result of inter-segment contagion.

In the WFZ space-time diagram (Figure 4), the tightest temporal cluster is four earthquakes between 620±30 and 1230±60 cal years B.P. The mean length of this cluster is 620 cal years. We use this time span to define a cluster for the purpose of the moving window test, acknowledging that the cluster could be several hundred years longer or shorter. The effect of this approximation on the moving window method is straightforward. If clusters were defined more restrictively (e.g., four earthquakes in 520 years), then there would be fewer of them in the synthetic composite history, and conversely, clusters defined less restrictively (e.g., four earthquakes in 704 years) would be more abundant. The same argument can be made for defining gaps, which we define at 900 cal years based on the earthquake gap between 1230±60 and 2130±100 cal years B.P. The remainder of the observed WFZ space-time diagram contains no obvious clusters or gaps tighter than those defined above.

Having now defined the cluster and gap combinations to test against, we construct 5.6-kyr time windows (the length of the WFZ observed record) on all the 12 synthetic composite paleoseismic histories to see how often these combinations appear. Windows were moved at 1-kyr increments down the composite histories; thus each model contains 350-400 windows. At each window position, we record the number of clusters and gaps as previously defined. Each window may contain as few as no clusters and gaps (the least clustered combination) or as many as three clusters and three gaps (the most clustered combination observed). In the 12 models (results of models 1-4 are shown in Figure 6) we observed 19 different combinations of clusters and gaps (some possible permutations were never observed), which are numbered from least to most clustered in Table 5. The observed WFZ history contains one cluster and one gap (combination 5 in Table 5), so the combinations listed in Table 5 with numbers greater than 5 are more "clustered" than the observed WFZ history.

Results of the Moving Window Test

The most common cluster/gap combination observed in 4 of the 12 synthetic composite models was one cluster and one gap (10%-26% of all windows had this combination), which is the pattern in the observed WFZ record (Figure 4). Therefore one could say that the earthquake pattern in the observed WFZ record has a 10-26% chance of representing a composite history created only by random actions among five segments (rather than by contagion). However, the synthetic composite histories typically contained combinations that are more clustered than that observed for the WFZ (i.e., combinations 6-19 in Table 5). By including the frequency of occurrence of these more clustered combinations, we can state that for the models we considered, there is a 18-69% chance (Table 5) of obtaining a composite history as clustered or more clustered than the observed WFZ history by purely random events on five independent fault segments. With probabilities centered around 50%, there is about an equal chance that the observed clustering in the WFZ space-time diagram was caused by chance or by intersegment contagion.

Table 5. Summary of Frequencies of Occurrence of Various Cluster/Gap Combinations in 100 Windows in Each Composite Synthetic Paleoseismic History

		Model[a]											
		1	2	3	4	5	6	7	8	9	10	11	12
Distribution		Poisson	Poisson	normal	normal	normal	normal	lognormal	lognormal	lognormal	lognormal	Weibull	Weibull
Mean recurrence,[b] years		obs	2000	obs	obs	2000	2000	obs	obs	2000	2000	2000	2000
COV[c]		1.0	1.0	0.3	0.5	0.3	0.5	0.2	0.5	0.2	0.5	3.5[d]	2.0[d]
Comb.[e]	No.[f]	Model[g]											
		1	2	3	4	5	6	7	8	9	10	11	12
0/0	1	6	8	20	13	26	9	27	31	25	19	25	10
0/1	2	13	12	24	17	13	16	27	29	13	31	7	7
1/0	3	8	9	14	15	14	15	9	7	12	2	25	30
0/2	4	5	4	5	1	2	3	7	15	4	9	0	1
1/1	5	22	26	17	22	21	24	13	10	12	21	14	17
2/0	6	7	5	1	5	5	7	2	1	2	0	7	18
0/3	7	0	0	0	0	1	0	0	0	0	1	0	0
1/2	8	11	14	8	5	5	6	4	6	7	10	1	4
2/1	9	13	9	6	14	7	7	10	0	5	5	11	9
3/0	10	5	5	0	0	0	1	0	0	0	0	1	2
0/4	11	0	0	0	0	0	0	0	0	0	0	0	0
1/3	12	2	1	0	1	2	2	2	0	2	1	0	0
2/2	13	0	4	6	4	4	5	0	1	10	1	4	0
3/1	14	5	1	1	1	0	2	0	0	2	0	1	3
4/0	15	2	0	0	0	0	0	0	0	0	0	1	0
2/3	16	0	0	0	0	0	0	0	0	1	0	0	0
3/2	17	2	0	0	1	1	2	0	0	4	0	2	0
4/1	18	0	1	0	0	0	0	0	0	0	0	0	0
3/3	19	0	0	0	0	0	1	0	0	0	0	1	0
Mean time[h] ycars		377	399	413	417	416	434	421	483	406	466	356	354
COV		1.03	1.03	0.84	0.84	0.87	1.02	0.78	0.84	0.83	0.82	0.82	0.84
Percent cluster[i]		17	15	7	10	8	13	5	3	8	5	10	12
Percent gaps[j]		8	8	7	7	6	7	6	9	8	9	4	3
>WFZ[k]		69	66	39	54	45	57	31	18	45	39	52	53

Frequency of occurrence given in percent. Poisson mean = 67.5%, normal mean = 48.8%, lognormal mean = 33.0%, and Weibull mean = 52.5%.

[a] Parameters of the individual synthetic histories.

[b] The mean recurrence interval used to generate the 200 recurrence times for the individual synthetic paleoseismic history of each fault segment; obs indicates that the weighted mean return time for the past 5.6 kyr (from Table 3) was used for each segment; 2000 indicates that all five modeled segments were assumed to have the same mean recurrence time of 2000 yr.

[c] COV, coefficient of variance, of recurrence interval used to generate the 200 recurrence times for the individual synthetic paleoseismic history of each fault segment. This COV defined the variance of the distributions of recurrence time that were generated by the computer program STATMOST.

[d] These values are the shape parameter (β) of the Weibull distribution.

[e] Cluster/gap combination, given as the number of clusters/number of gaps.

[f] Numbers of various unique combinations of clusters and gaps; also used in text.

[g] Characteristics of the composite synthetic histories.

[h] Mean interevent time in the composite history.

[i] Number of clusters divided by the total number of earthquakes in the composite history

[j] Number of gaps divided by the total number of earthquakes in the composite history

[k] The percentage of all windows comprised by cluster/gap combinations 5-19 (as or more clustered than the WFZ record).

Because contagion does not appear necessary to produce the observed clustering, we calculate the probabilities of future earthquakes on fault segments (next section) as if each segment behaves independently.

The coefficient of variation of composite interevent times in the WFZ space-time diagram (0.66) is significantly lower than that in any of the synthetic composite histories. This pattern suggests that some mechanism may be regulating the occurrence of large earthquakes at quasi-periodic intervals along the entire length of the WFZ but without producing a clear spatial pattern of rupture migration among segments (Figure 4).

Multisegment Ruptures

Inspection of the space-time diagram (Figure 4) shows a number of cases where the dates for earthquakes on adjacent segments overlap. An alternate explanation to contagion (where an earthquake on one segment soon induces earthquakes on adjacent segments) is that these overlapping earthquakes are single events that ruptured two or more adjacent segments at the same time. Examples in Figure 4 include events X and Y on the Brigham City and Weber segments (~4600 and 3400 years B.P., respectively) and events W and X on the Salt Lake City and Provo segments at ~5200 years B.P. As seen by the heights of the error boxes on Figure 4, the dates of these events have uncertainties of the order of 300-500 years. The size of these uncertainties precludes the unequivocal correlation of these earthquakes as the same event. Until more precise dating is available to evaluate this possibility, the "megaquake" hypothesis needs to be considered as a valid end member scenario for planning purposes along the WFZ.

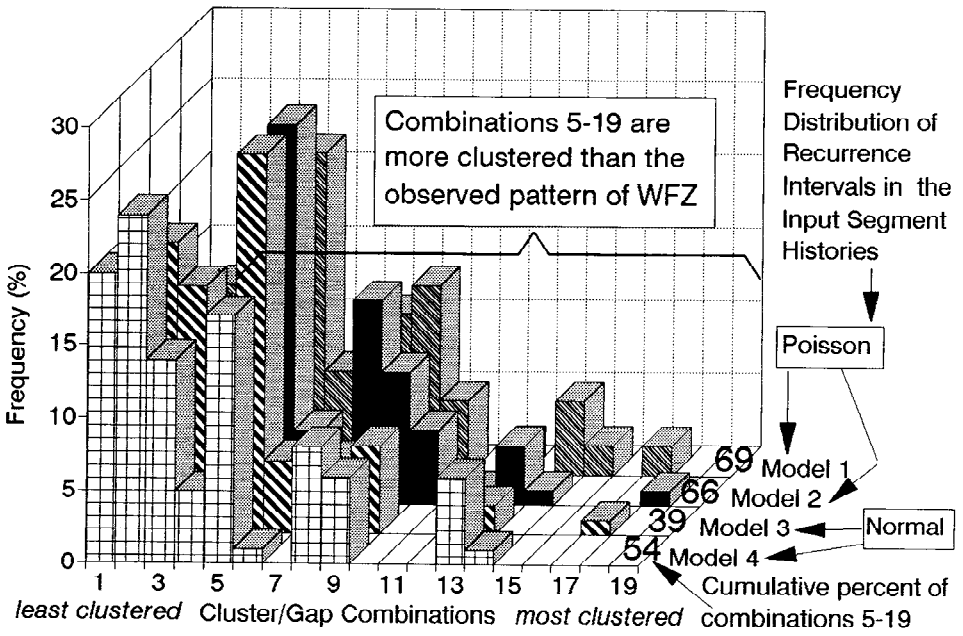

Figure 6. Frequency of cluster/gap combinations found in 100 5.6-kyr time windows in models 1-4 (for model parameters, see Table 5). Cluster/gap combinations 1-19 on the horizontal axis reflect how "clustered" in time are earthquakes in the 5.6-kyr span of the window, as opposed to being uniformly spread through that time span. Observed permutations range from no clusters or gaps in the window (combination 1, least clustered; i.e., the earthquakes are very regularly spaced throughout the time window) to as many as three clusters and three gaps in the window (combination 19, most clustered; all the earthquakes in the window occur in clusters). The cumulative frequency of windows in the synthetic models that contain earthquake patterns at least as clustered as the observed WFZ window (i.e., one cluster and one gap; combination 5) ranges from 39% to 69% for these models. This means that the observed WFZ "temporal clustering" could easily be produced by chance patterns among independent segments, assuming that the model input parameters accurately reflect the behavior of WFZ fault segments. Results of the other eight models are given in Table 5.

Probabilities for Future Large Earthquakes

The available seismological and geological data for the WFZ allow three direct approaches for estimating probability of future large earthquakes: regional, fault-specific, and segment-specific. The regional probabilities are based on instrumental data from the Wasatch Front region, whereas the fault- and segment-specific estimates are based entirely on the paleoseismic record of the WFZ. Previously, *Cluff et al.* [1980] used early paleoseismic data from the Provo (Hobble Creek site) and Weber (Kaysville site) segments and a semi-Markov model to estimate the probabilities for large earthquakes along the WFZ. *Youngs et al.* [1987, 1988] estimated probabilities for large earthquakes from recurrence intervals calculated by dividing inferred displacements per event by the rate of fault motion. *Nishenko and Schwartz* [1990] and *Nishenko* [1992] used direct observations of recurrence intervals from the paleoseismic data available at that time to estimate probabilities for the WFZ based on both renewal and Poisson models. They concluded that the Brigham City segment has an elevated probability with respect to the other segments. Here we update these earlier estimates using additional data collected since 1990 and introduce objective criteria for data selection and analysis.

Regional Probabilities

Seismographic network coverage of the Wasatch Front and Intermountain Seismic Belt in Utah provides a regional perspective of large earthquake activity that is independent of the geologic record shown in Figure 4. The Wasatch Front recurrence model of *Arabasz et al.* [1992] is based on instrumental data from 1962 to 1985 for earthquakes between $2<M_L<6$ in a 85,000 km^2 region centered on the WFZ. Extrapolating the occurrence rate of these smaller earthquakes to larger $M>7$ earthquakes indicates return times of 280 years (1σ confidence limit between 120 and 630 years) in the Wasatch Front region [*Arabasz et al.*, 1992, p. D23].

The Wasatch Front area includes 28 late Quaternary fault zones, in addition to the WFZ [*Hecker*, 1993, p. 15], and we assume that the combined hazard estimate due to earthquakes from these sources can be realistically described as a Poisson process with an exponential distribution of interevent times and a hazard function that is independent of the length of time since the last event [*Cornell and Toro*, 1992]. The probability of an event during a time interval, $t+\Delta t$, given that the last event occurred t years ago, is:

$$F_{(t)} = 1 - e^{-(\lambda \Delta T)} \quad (3)$$

where λ is the annual rate of occurrence and Δt is the length of the exposure period in years. In this study, Δt is 20, 50, or 100 years.

These types of estimates are useful for regional hazards assessments and the definition of baseline hazard levels for building code development and seismic zonation [e.g., *Cornell and Winterstein*, 1988; *Gori and Hays*, 1992]. Additionally, they provide a frame of reference for comparison with the time-varying probability estimates discussed in the

next section. Based on the *Arabasz et al.* [1992] recurrence model for earthquakes of $M>7$ along the Wasatch Front, the Poisson probability ranges from 0.16 (0.076 to 0.34 at 1σ) for a 50-year exposure time to 0.30 (0.15 to 0.56 at 1σ) for a 100-year exposure time.

Fault Specific Probabilities

As seen on Figure 4, there have been 16 $M>7$ earthquakes along the WFZ in the past ~5600 years (limited by the age of event X on the Salt Lake City segment, at 5244-5749 cal years B.P.). The average interevent time (328-359 years, with a preferred median value of 350 years) is similar to the previously cited average composite recurrence interval of 395±60 years (based on 15 earthquakes in the past 7 kyr [*Machette et al.*, 1992a] but is shorter than the 444-to 666-year recurrence interval of *Schwartz and Coppersmith* [1984], based on 12 to 18 earthquakes in the past 8 kyr.

If this sequence of events can be described as a Poisson process, the 350-year recurrence interval results in probabilities of 0.13 and 0.25 for 50- and 100-year exposure periods. These probabilities are similar to the 0.12 (50-year) and 0.22 (100-year) probabilities estimated by *Nishenko and Schwartz* [1990] before the discovery of event Z on the Brigham City segment [*McCalpin and Forman*, 1993] and events Y and X on the Salt Lake City segment [*Lund*, 1992; *Black et al.*, 1995].

The confidence limits for the above interevent time estimate (16 events in 5600 years) are 10.04 and 24.3 events in 5600 years at the 10% significance level (or interevent times of 557.8 and 230.4 years, respectively). (See tables of confidence limits for the expected value of a Poisson distribution in the work by *Pearson and Hartley* [1956] and *Beyer* [1985]). In other words, the probabilities at the 0.05 and 0.95 confidence limits for a 50-year exposure period are 0.086 and 0.195, respectively, and are 0.164 and 0.352 for a 100-year exposure period, respectively. These latter values are shown in Figure 7.

WFZ probabilities based on the paleoseismic record (0.13, 0.25) are only slightly less than the probabilities for the entire Wasatch Front region (0.16, 0.30) extrapolated from historic seismicity. The latter includes contributions from the other 28 late Pleistocene and Holocene faults in the Wasatch Front region. *Hecker* [1993, p. 12] suggests that only half of the surface-rupturing earthquakes during the past 15 kyr in the Wasatch Front region occurred on the WFZ.

Segment Specific Probabilities

Do large earthquakes occur randomly in space and time on individual fault segments, or is their occurrence modulated by some type of cyclic or periodic behavior, as *Gilbert* [1884] hypothesized? Recent studies have examined the distribution of earthquake recurrence times in interplate environments [*Nishenko and Buland*, 1987; *Savage*, 1994; *Ward*, 1991, 1992; *WGCEP*, 1988, 1990]. For intraplate environments, there have been few data to unequivocally define a recurrence time distribution for any particular fault or fault segment. Hence most probability estimates in intraplate regions assume

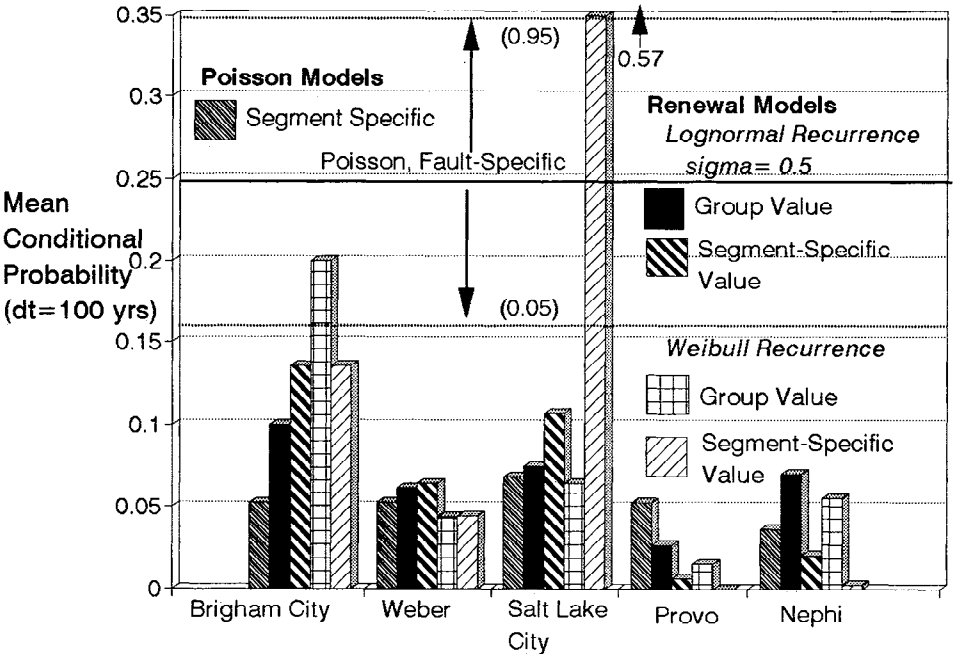

Figure 7. Conditional probability estimates for M>7 earthquakes along the central Wasatch fault zone, Utah. Four time-dependent (renewal) probability estimates for a 100-year exposure period along the central WFZ are shown: group and segment-specific lognormal (with COV=0.5) and group and segment-specific Weibull. In each case the height of the bar is equal to the mean probability estimate as listed in table 6. The fault and segment-specific Poisson estimates are also shown for reference. 90% confidence intervals for the fault-specific Poisson estimate are shown as dotted lines labeled 0.05 and 0.95. The Weber, Provo, and Nephi segments have renewal estimates that are less than or equal to the segment-specific and fault-specific Poisson estimates. The Salt Lake City and Brigham City segments have probability estimates that are greater than or equal to the segment-specific estimate and, for some model combinations, equal to the fault-specific Poisson estimate. See Table 6 for additional model parameters.

a Poisson process (as described in preceding sections). Time-dependent recurrence distributions for intraplate earthquakes were discussed by *Johnston and Nava* [1985] for the New Madrid region, but the distribution parameters were based on historic and instrumental seismicity. Can the 5.6-kyr data base shown in Figure 4 provide any empirical constraints on the frequency distribution of earthquake return times in an intraplate environment?

The small number of observed recurrence intervals from individual fault segments (1 to 3) during the past 5.6 kyr precludes the unequivocal demonstration of a particular type of recurrence behavior (i.e., random versus periodic). To establish a baseline for comparing other probability models, we computed segment-specific probability estimates based on a Poisson model and associated 90% confidence limits for the mean recurrence time based on the number of observed earthquakes (2 to 4) on each segment in the past 5.6 ka (Table 6, Poisson models, segment- specific).

An alternate approach is to pool all the available data for the WFZ segments and empirically fit these observations to some standard recurrence time distributions. By grouping these data, we assume that these recurrence intervals are all members of the same population. This approach has been used to characterize the recurrence distribution of plate boundary earthquakes [*Rikitake*, 1976; *Nishenko*, 1985; *Jacob*, 1984). Two families of distributions, Weibull and lognormal, were chosen for our estimates. The lognormal distribution is characterized by a "heavy" right-hand tail and favors longer-than-average return times. In contrast, the Weibull distribution is more flexible and can represent a number of different failure time distributions by varying the shape parameter, β. A β of 1 is the exponential distribution and β=2 is the Rayleigh distribution. For β=3.5 the distribution is approximately symmetrical (i.e., approximates the normal distribution).

We fitted the grouped data to a Weibull distribution, following the procedures outlined by *Nishenko* [1985]. Since these data represent a sample from a much longer time series, we used a $(n_i\text{-}1/2)/N$ rank distribution to construct the empirical cumulative distribution function F(t). The cumulative distribution is defined as

$$F(t) = 1 - \exp(-t/\theta)^{\beta} \quad (4)$$

where t is the elapsed time, β is the Weibull shape parameter or slope, and 0 is the characteristic life (i.e., the point at which failure prior to θ is equal to 1/e). The characteristic life θ is related to the mean recurrence time μ by $\mu = \theta\ \Gamma\ (1+1/\beta)$ [*Kapur and Lamberson*, 1977]. Taking the double natural logarithm of $F(t)$ yields a linear equation that can be solved for the slope β and intercept β ln θ. A plot of ln ln $[1/(1\text{-}F(t))]$ versus ln T for the entire grouped data repeat time history of the central WFZ has a least-squares fit to the slope or shape parameter β = 3.36 and a mean recurrence time, μ= 1775±491 years at 2σ (Figure 8a). Confidence intervals (labeled 0.05 and 0.95) are shown for the Weibull fit to the data (see *Kapur and Lamberson* [1977, p. 308-311] for a discussion of this technique).

Inspection of Figure 8a suggests that there may be two separate populations of recurrence times along the WFZ, short-recurrence (~1300 years) and long-recurrence (~2300 years). Accordingly, we split the data at ln T=7.5 and replotted the short and long groups in Figure 8b. These new fits have better correlation coefficients and steeper slopes than the grouped data (β= 17.8 and 8.3 versus 3.36 in the grouped set). The mean recurrence times for the short and long groups are 1328±104 and 2346±448 years, respectively (ranges are 2 σ).

All three Weibull distributions in Figure 8 were used to develop probability estimates for the central WFZ (Table 6). For the Brigham City, Provo, and Nephi segments, we chose the group and long-recurrence distributions for our estimates. In the case of the Nephi and Provo segments, this choice is based on similarities with the observed recurrence times (2716 and 2297 years, respectively, versus group and "long" Weibull average repeat times of 1775 and 2346 years, respectively).

In the case of the Brigham City segment, the choice of distribution is more critical. As seen in Figure 4, the observed Holocene recurrence times range from 1240 to 1330 years, which would appear to favor the "short" Weibull recurrence model with a mean repeat time of 1328 years. The fact that the current elapsed time is 2125 years is, however, problematic. The elapsed time is not merely one or two standard deviations beyond the mean recurrence but is equivalent to nearly two full recurrence times. The extreme length of the current elapsed time, however, does not appear to be due to undiscovered events younger than 2125 years B.P. [*McCalpin and Forman*, 1993]. If we assume a "short" Weibull recurrence model, then the probabilities are >>0.99, regardless of the length of the exposure window. Since the observed elapsed time is now closer to the mean of the long Weibull model (2125 versus 2346 years, respectively), we chose to use the long model for our estimates. If we consider the current elapsed time as a quasi-recurrence interval and add it to the other Holocene recurrence intervals for the Brigham City segment, the mean recurrence time increases toward the value for the group Weibull model (1775 years)(see Table 6).

Both the Weber and Salt Lake City segments have Holocene recurrence intervals that range from 1138 to 2048 years and 1268 to 1441 years, respectively. Accordingly, we used the group and short-recurrence times in our calculations for those segments (Table 6).

Probability estimates for the central segments of the WFZ were also computed using a lognormal distribution. As in the case of the Weibull distribution, we grouped all of the recurrence times into a single distribution (labeled "group" in Table 6) with mean recurrence time of 1767 years. The uncertainty in the recurrence time, at the 90% confidence limit, is 1.645 Var $(T_{exp})^{1/2}$, where T_{exp} is the expected value of the mean recurrence, and the variance of T_{exp} is a function of both the sample variance and the intrinsic variability σ_D [*Nishenko and Buland*, 1987, p. 1389]. Intrinsic variability is a parameter to describe the natural variation of recurrence intervals and is independent of the errors or reliability in estimating the length of the recurrence interval. Probabilities were calculated using two values of intrinsic variability, σ_D= 0.21 and 0.5. The value of σ_D= 0.21 is taken from the global study of *Nishenko and Buland* [1987]. The value σ_D= 0.5 is used to provide an intermediate step between periodic behavior (σ_D< 0.2) and the more irregular recurrence behavior typified by the exponential distribution (σ_D= 1). Segment-specific estimates, using the observed recurrence times from individual segments rather than the group average, were also computed using the two values of σ_D (labeled segment in Table 6).

Table 6. Wasatch Fault Zone Probability Estimates

				Conditional Probability (a)					
				Poisson Models					
		Repeat Time, years (b)		20 Years		50 Years		100 Years	
Fault Specific									
16 events/5.6 ka		350 (230.4 - 557.8)		0.055 (0.035 - 0.083)		0.13 (0.086 - 0.195)		0.248 (0.16 - 0.35)	
Segment Specific									
3 events / 5.6 ka	Brigham City	1867 (722.6-6846)		0.01 (0.003-0.027)		0.026 (0.007-0.066)		0.052 (0.014-0.129)	
3 events / 5.6 ka	Weber	1867 (722.6-6846)		0.01 (0.003-0.027)		0.026 (0.007-0.066)		0.052 (0.014-0.129)	
4 events / 5.6 ka	Salt Lake City	1400(612-4088)		0.014 (0.005-0.032)		0.035 (0.012-0.078)		0.068(0.024-0.151)	
3 events / 5.6 ka	Provo	1867 (722.6-6846)		0.01 (0.003-0.027)		0.026 (0.007-0.066)		0.052 (0.014-0.129)	
2 events / 5.6 ka	Nephi	2800(889-15745)		0.007(0.001-0.022)		0.017(0.003-0.055)		0.035(0.006-0.106)	
				Lognormal Renewal Models					
		Repeat Time, years	Elapsed Time, years B.P. (c)	20 Years		50 Years		100 Years	
				σ = 0.21	σ = 0.5	σ = 0.21	σ = 0.5	σ = 0.21	σ = 0.5
Group	Brigham City	1767	2125 ±104	0.069 (0.053-0.088)	0.021 (0.015-0.029)	0.164 (0.128-0.207)	0.051 (0.037-0.072)	0.305 (0.243-0.373)	0.10 (0.074-0.138)
	Weber	1767	1016 ± 62	0.004 (0.001-0.011)	0.012 (0.006-0.023)	0.01 (0.003-0.03)	0.03 (0.016-0.056)	0.025 (0.008-0.068)	0.061 (0.033-0.111)
	Salt Lake City	1767	1230 ± 62	0.014 (0.006-0.029)	0.015 (0.009-0.026)	0.037 (0.016-0.075)	0.037 (0.022-0.063)	0.081 (0.037-0.155)	0.075 (0.045-0.124)
	Provo	1767	618 ± 30	0.0 (0.0-0.0)	0.004 (0.002-0.012)	0.0 (0.0-0.0)	0.012 (0.005-0.032)	0.0 (0.0-0.001)	0.026 (0.01-0.067)
	Nephi	1767	1148 ± 68	0.009 (0.003-0.022)	0.014 (0.008-0.025)	0.025 (0.01-0.057)	0.035 (0.02-0.061)	0.056 (0.023-0.121)	0.07 (0.041-0.120)
Segment	Brigham City	1275	2125 ±104	0.115 (0.077-0.163)	0.029 (0.016-0.056)	0.263 (0.184-0.361)	0.07 (0.04-0.134)	0.459 (0.337-0.591)	0.135 (0.079-0.249)
	Weber	1693	1016 ± 62	0.005 (0.0-0.038)	0.013 (0.003-0.052)	0.013 (0.001-0.097)	0.032 (0.008-0.125)	0.032 (0.003-0.199)	0.064 (0.017-0.235)
	Salt Lake City	1384	1230 ± 62	0.045 (0.016-0.098)	0.022 (0.01-0.05)	0.111 (0.042-0.23)	0.054 (0.25-0.121)	0.221 (0.09-0.415)	0.107 (0.05-0.228)
	Provo	2432	618 ± 30	0.0 (0.0-0.0)	0.001 (0.0-0.021)	0.0 (0.0-0.0)	0.002 (0.0-0.054)	0.0 (0.0-0.0)	0.006 (0.0-0.109)
	Nephi	2716	1148 ± 68	0.0 (0.0-0.008)	0.004 (0.0-0.072)	0.0 (0.0-0.022)	0.01 (0.001-0.171)	0.0 (0.0-0.051)	0.02 (0.001-0.311)
				Weibull Renewal Models					
		Repeat Time, years (b)	Elapsed Time, years B.P. (c)	20 Years		50 Years		100 Years	
Group	Brigham City	1775 ± 491	2125 ±104	0.042 (0.029-0.044)		0.103 (0.071-0.108)		0.20 (0.143-0.207)	
	Weber	1775 ± 491	1016 ± 62	0.008 (0.002-0.019)		0.02 (0.006-0.047)		0.043 (0.012-0.093)	
	Salt Lake City	1775 ± 491	1230 ± 62	0.012(0.004-0.023)		0.031 (0.011-0.058)		0.064 (0.024-0.115)	
	Provo	1775 ± 491	618 ± 30	0.003 (0.0-0.010)		0.007 (0.001-0.027)		0.015 (0.003-0.055)	
	Nephi	1775 ± 491	1148 ± 68	0.010 (0.003-0.021)		0.027 (0.009-0.053)		0.055 (0.019-0.107)	
Segment	Brigham City	2346 ± 448	2125 ±104	0.025 (0.005-0.053)		0.065 (0.013-0.130)		0.136 (0.029-0.255)	
	Weber	1328 ± 104	1016 ± 62	0.004 (0.0-0.025)		0.014 (0.001-0.071)		0.044 (0.004-0.172)	
	Salt Lake City	1328 ± 104	1230 ± 62	0.090 (0.023-0.145)		0.252 (0.075-0.357)		0.568 (0.238-0.663)	
	Provo	2346 ± 448	618 ± 30	0.0 (0.0-0.0)		0.0 (0.0-0.001)		0.0 (0.0-0.002)	
	Nephi	2346 ± 448	1148 ± 68	0.0 (0.0-0.004)		0.001 (0.0-0.01)		0.002 (0.0-0.023)	

a- 90% confidence interval in parentheses b- Repeat time ± 2 sigma c- Elapsed time ± 2 sigma

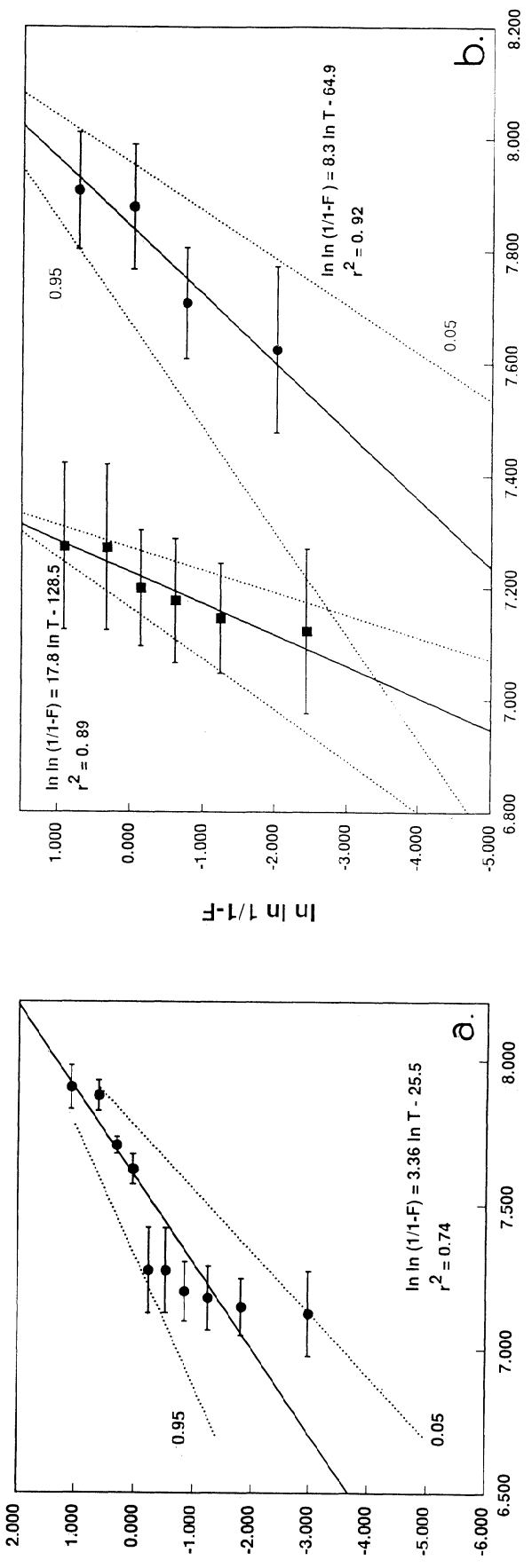

Figure 8. Cumulative Weibull plots of ln ln [1/ 1-$F(T)$] versus ln T for Holocene earthquake repeat times along the central five segments of the WFZ. Horizontal error bars shown for interevent times are 90% confidence intervals (see Table 6). Cumulative distributions are plotted according to a (n_T-1/2)/N plotting rule. Least squares fit to the data (solid lines) define the Weibull distribution parameters. Dotted lines show 0.05 and 0.95 confidence interval estimates to the distribution. (a) All interevent times in the past 5.6 kyr (grouped data); β=3.36, mean repeat time=1775±291 years (2σ range). Two subgroups of interevent times appear, those with ln T<7.5 and ln T>7.5, suggesting bimodal recurrence behavior. (b) Data from Figure 8a replotted to emphasize the short-recurrence (ln T<7.5) and long-recurrence (ln T>7.5) groups. For the short-recurrence group, β=17.8 and mean repeat time=1328±104 years (2σ range). For the long-recurrence group, β=8.3 and mean repeat time=2346±448 years (2σ range).

Figure 7 compares a suite of conditional probability estimates for a 100-year exposure window along the WFZ. Four time-dependent (renewal) probability estimates for the five WFZ segments are compared: group and segment-specific lognormal (with σ_D= 0.5) and group and segment-specific Weibull. In each case, the height of the bar is equal to the mean probability estimate for the model as listed in Table 6. The fault- and segment-specific Poisson-based estimates are also shown for reference.

Overall, the Weber, Provo, and Nephi segments have low probabilities regardless of the model chosen. For the time-dependent models, these low values reflect the recency of faulting. The last earthquakes on these segments occurred ~620 (Provo), 1020 (Weber) and 1150 (Nephi) years B.P., compared to segment-specific mean recurrence times of ~2300 (Provo), 1780 (Weber), and 2720 (Nephi) years. In other words, the elapsed times are between 0.27 and 0.57 of the estimated mean repeat time.

The ratio of time-dependent (or renewal) to Poisson probabilities provides another comparison of the hazard level on these segments. The Provo segment has time-dependent probabilities (0.01-0.026) that are less than half the segment-specific Poisson estimate (0.05). Both the Weber and Nephi segments have renewal probabilities that are similar to the segment-specific Poisson probabilities (0.03-0.05). In Figure 7, all three segments display time-dependent probabilities that are considerably less than 0.16, the 0.05 confidence limit for the fault-specific Poisson model. In other words, if the Provo, Weber, and Nephi segments produce characteristic earthquakes quasi-periodically, then the hazard level for these segments in the next 100 years is less than or equal to the hazard if large earthquakes were assumed to occur randomly.

In contrast, both the Salt Lake City and Brigham City segments have time-dependent probabilities (Table 6) that are greater than or equal to their segment-specific Poisson estimates (0.05 and 0.07, respectively). The elapsed time for Salt Lake City (1275 years) is approximately equal to the mean repeat times for the Weibull and lognormal segment-specific models (1328 and 1384 years) and is 0.72 of the group repeat times (1767 and 1775 years). The largest probability in Figure 7 (0.57) comes from the short Weibull recurrence model (T= 1328±104 years), which has an extremely small COV (0.04). The segment-specific lognormal model, with σ_D= 0.5, is much broader, has a larger coefficient of variation (0.68), and a smaller hazard estimate (0.11).

As discussed previously, the recurrence history for the Brigham City segment is problematic. While additional trenching on the Brigham City segment has improved the paleoearthquake chronology [*McCalpin and Forman*, 1993], the current longer-than-average elapsed time is discordant with the quasi-periodic earthquake model and the Holocene earthquake history. The use of group and long Weibull recurrence times is suggested by this longer-than-average elapsed time, and this choice results in conditional probabilities that are 2.5 to 4 times larger than the segment-specific Poisson values. The group and segment-specific lognormal values are also 2 to 2.7 times larger than the Poisson values. In other words, both the Salt Lake City and Brigham City segments have time-dependent hazard levels for M>7 earthquakes in the next 100 years that are greater than if large earthquakes were assumed to occur randomly.

Discussion

The justification for performing over two decades of paleoseismic trenching and dating on the WFZ was that the historic seismic record was too short to adequately assess the future hazard from large (M>7) surface-rupturing earthquakes [*Schwartz and Coppersmith*, 1984]. Our analysis confirms this supposition and highlights some major differences between the hazard predicted by paleoseismic versus historic seismic data for certain fault segments. These discussions have focused only on the hazard due to M>7 earthquakes on the WFZ and have not included the hazard due to smaller, but still potentially damaging earthquakes that can occur anywhere within the Wasatch Front region.

Synthetic modeling indicates that apparent temporal cluster(s) of earthquakes observed in the past 1.5 kyr have a 18-69% chance of arising from random actions of independent fault segments, so our probability estimates do not account for any contagion effects. Uncertainties in earthquake age of 300-500 years preclude the unambiguous identification of multisegment "megaquakes", and age overlaps could also be due to temporal coincidence.

Three of the five central segments (Weber, Provo, Nephi) have had large earthquakes fairly recently, and all of the renewal models examined estimate relatively low probabilities for M>7 earthquakes in the near future. For the Brigham City and Salt Lake City segments, the renewal model estimates are considerably higher. In the case of the Salt Lake City, this reflects the fact that the current elapsed time is near the average repeat time for M>7 events during the Holocene. For Brigham City, however, the elapsed time is considerably longer than the observed recurrence intervals in the late Holocene. This discrepancy signals caution to the conclusion that all fault segments along the WFZ may behave in the same manner.

Acknowledgements. W.R. Lund, D.A. Ostenaa, and S.L. Forman kindly provided unpublished numerical ages from WFZ trench sites. D.M. Perkins suggested some of the techniques used in synthetic modeling, and A.R. Nelson and C. Bufe added insightful comments in review. This paper benefitted from thorough reviews by G. P. Biasi, A.J. Crone, S. Hecker, A.R. Nelson, C. S. Prentice, D.P. Schwartz, and one anonymous reviewer. This study was supported jointly by the GEO-HAZ Research and Development Fund and by the U.S. Geological Survey National Earthquake Hazard Reduction Program.

References

Arabasz, W.J., J.C. Pechmann, and E.D. Brown, Observational seismology and evaluation of earthquake hazards and risk in the Wasatch Front area, Utah, in *Assessment of Regional and Earthquake Hazards and Risk Along the Wasatch Front, Utah*, edited by P.L. Gori and W.W. Hays, *U.S. Geol. Surv. Prof. Pap. 1500-D*, D1-D36, 1992.

Bakun, W.H., and A.G. Lindh, The Parkfield, California earthquake prediction experiment, *Science, 229*, 619-624, 1985.

Berger, G.W., Dating Quaternary events by luminescence, in *Dating Quaternary Sediments*, edited by D.J. Easterbrook, *Spec. Pap. 227, Geol. Soc. Am.*, 13-50, 1988.

Beyer, W.H., *CRC Handbook of Tables for Probability and Statistics*, 2nd ed., CRC Press, Boca Raton, Fla., 1985.

Black, B.D., and W.R. Lund, Timing of large earthquakes on the Salt Lake City segment of the Wasatch fault zone--New information from the South Fork Dry Creek site, Salt Lake County, Utah, *Geol. Soc. Am. Abstr. Programs, 27*(4), 3, 1995.

Black, B.D., W.R. Lund and B.H. Mayes, Summary of new information from the South Fork Dry Creek site, Salt Lake County, Utah, in *Environmental and Engineering Geology of the Wasatch Front Region*, edited by W.R. Lund, *Utah Geol. Assoc. Pub. 24*, 11-30, 1995.

Brillinger, D.R., Some bounds for seismic risk, *Bull. Seismol. Soc. Am., 72*, 1403-1410, 1982.

Cluff, L.S., A.S. Patwardhan, and K.J. Coppersmith, Estimating the probability of occurrences of surface faulting on the wasatch fault zone, Utah, *Bull. Seismol. Soc. Am., 70*, 1463-1478, 1980.

Cornell, C.A., and G. Toro, Seismic hazard assessment, in *Techniques for Determining Probabilities of Geologic Events and Processes*, Stud. Math. Geol., no. 4, edited by R.L. Hunter and C.J. Mann, pp.147-166, Oxford Univ. Press, New York, 1992.

Cornell, C.A., and S.R. Winterstein, Temporal and magnitude dependence in earthquake recurrence models, *Bull. Seismol. Soc. Am.*, 78, 1522-1537, 1988.

Cornell, C.A., S.-C. Wu, and S.R. Winterstein, Seismic hazard induced by mechanically interactive fault segment, *Bull. Seismol. Soc. Am., 83*, 436-449, 1993.

Crone, A.J., M.N. Machette, M.G. Bonilla, J.J. Lienkaemper, K.L. Pierce, K.L., W.E. Scott, and R.C. Bucknam, Surface faulting accompanying the Borah Peak earthquake and segmentation of the Lost River fault, central Idaho, *Bull. Seismol. Soc. Am., 77*, 739-770, 1987.

Forman, S. L., M. N. Machette, M. E. Jackson,and P. Maat, An evaluation of thermoluminescence dating of paleoearthquakes on the American Fork segment, Wasatch fault zone, Utah, *J. Geophys. Res., 94*, 1622-1630, 1989.

Forman, S.L., A.R. Nelson, and J.P. McCalpin, Thermoluminescence dating of fault-scarp derived colluvium: Deciphering the timing of paleoearthquakes on the Weber segment of the Wasatch fault zone, north central Utah, *J. Geophys. Res., 96*, 595-605, 1991.

Geyh, A.A., and H. Schleicher, *Absolute Age Determination*, Springer-Verlag, New York, 1990.

Gilbert, G.K., A theory of the earthquakes of the Great Basin, with a practical application, *Am. J. Sci., 27*, 49-53, 1884.

Gori, P.L. and W.W. Hays (Eds.), Assessment of regional earthquake hazards and risk along the Wasatch Front, Utah: *U.S. Geol. Surv. Prof. Pap. 1500-A-J*, 1992.

Hanson, K.L., and D.P. Schwartz, Guidebook to late Pleistocene and Holocene faulting along the Wasatch Front and vicinity-Little Cottonwood Canyon to Scipio, Utah, paper presented at Chapman Conference on Fault Behavior and the Earthquake Generation Process, AGU, Snowbird, Utah, 1982.

Hecker, S., Quaternary tectonics of Utah with emphasis on earthquake-hazard characterization, *Utah Geol. Surv. Bull., 127*, 157 pp., 1993.

Huntley, D.J., G.W. Berger, W.M.R. Divigalpitaya, and T.A. Brown, Thermoluminescence dating of sediment, *J. Eur. Stud. Group Phys. Chem. Math. Tech. Appl. Archaeol., 9*, 607-618, 1983.

Jackson, M., The number and timing of Holocene paleoseismic events on the Nephi and Levan segments, Wasatch fault zone, Utah, *Utah Geol. Surv. Spec. Stud., 78*, 23 pp., 1991.

Jacob, K.H., Estimates of long-term probabilities for future great earthquakes in the Aleutians, *Geophys. Res. Lett., 11*, 295-298, 1984.

Johnston, A.C., and S.J. Nava, Recurrence rates and probability estimates for the New Madrid seismic zone, *J. Geophys. Res., 90*, 6737-6753, 1985.

Kapur, K.C., and L.R. Lamberson, *Reliability in Engineering Design*, 586 pp., John Wiley, New York, 1977.

Lay, T., and H. Kanamori, An asperity model of large earthquake sequences, in *Earthquake Prediction: An International Review, Maurice Ewing Ser., vol. 4*, edited by D.W. Simpson and P.G. Richards, pp. 579-592, AGU, Washington, D.C., 1981.

Lund, W.R., New information on timing of large earthquakes on the Salt Lake City segment of the Wasatch fault zone; implications for increased earthquake hazard along the central Wasatch Front, *Wasatch Front Forum, 8*(3), 12-13, 1992.

Lund, W.R., and D.P. Schwartz, Fault behavior and earthquake recurrence at the Dry Creek site, Salt Lake segment, Wasatch fault zone, Utah, *Geol. Soc. Am. Abstr. Programs 19*, 317, 1987.

Lund, W.R., B.D. Black, and D.P. Schwartz, Late Holocene displacement on the Provo segment of the Wasatch fault zone at Rock Canyon, Utah County, Utah, *Geol. Soc. Am., Abstr. Programs, 22*, 37, 1990.

Lund, W.R., D.P. Schwartz, W.E. Mulvey, K.E. Budding, and B.D. Black, Fault behavior and earthquake recurrence on the Provo segment of the Wasatch fault zone at Mapleton, Utah County, Utah, in *Paleoseismology of Utah*, vol. 1, *Utah Geol. Surv. Spec. Stud., 75*, 41 pp., 1991.

Machette, M.N., Documentation for benchmark photographs showing some effects of the 1983 Borah Peak earthquake with considerations for studies of scarp degradation, in *Proceedings of Workshop XXVIII on the Borah Peak earthquake, Idaho*, vol. A, edited by R.S. Stein and R.C. Bucknam, *U.S. Geol. Surv. Open File Rep., 85-290*, 97-109, 1985.

Machette, M.N. (Ed.), *In the Footsteps of G.K. Gilbert- Lake Bonneville and Neotectonics of the Eastern Basin and Range Province, Utah Geol. Min. Surv. Misc. Publ., 88-1*, 120 pp., 1988a.

Machette, M.N., American Fork Canyon-Holocene faulting, the Bonneville fan-delta complex, and evidence for the Keg Mountain oscillation, in *In the Footsteps of G.K. Gilbert- Lake Bonneville and Neotectonics of the Eastern Basin and Range Province*, edited by M.N. Machette, *Utah Geol. Min. Surv. Misc. Publ., 88-1*, 89-95, 1988b.

Machette, M.N., and W.R. Lund, Trenching across the American Fork segment of the Wasatch fault zone, Utah, *Geol. Soc. Am., Abstr. Programs, 19*, 317, 1987.

Machette, M.N., S.F. Personius, and A.R. Nelson, Quaternary geology along the Wasatch fault zone: segmentation, recent investigations, and preliminary conclusions, in *Evaluation of Urban and Regional Earthquake Hazard and Risk in Utah*, edited by P.L. Gori and W.W. Hays, *U.S. Geol. Surv. Open File Rep., 87-585*, A1-A72, 1987.

Machette, M.N., S.F. Personius, A.R. Nelson, D.P. Schwartz, and W.R. Lund, Segmentation and history of Holocene earthquakes, Wasatch fault zone, Utah, *J. Struct. Geol., 13*, 137-149, 1991.

Machette, M.N., S.F. Personius, and A.R. Nelson, Paleoseismology of the Wasatch fault zone: A summary of recent investigations, interpretations, and conclusions, in *Assessment of Regional Earthquake Hazards and Risk Along the Wasatch Front, Utah*, edited by P.L. Gori and W.W. Hays, *U.S. Geol. Surv. Prof. Pap. 1500-A*, A1-A71, 1992a.

Machette, M.N., S.F. Personius, and A.R. Nelson, The Wasatch fault zone, U.S.A., *Ann. Tectonicae, Spec. Issue, suppl. VI*, 5-39, 1992b.

McCalpin, J.P., Spatial/temporal patterns of Quaternary faulting in the southern limb of the Yellowstone-Snake River Plain seismic parabola, northeastern Basin and Range margin, *Geol. Soc. Am. Abstr. Programs, 25*, 117, 1993.

McCalpin, J.P. and S.L. Forman, Chronology of paleoearthquakes on the Wasatch fault zone by thermoluminescence (TL) dating, in *Summaries of Technical Reports*, vol. XXVI, *U.S. Geol. Surv. Open File Rep., 88-434*, 506-511, 1988.

McCalpin, J.P., and S.L. Forman, Quaternary faulting and thermoluminescence dating of the East Cache fault zone, north-central Utah, *Bull. Seismol. Soc. Am., 81*, 139-161, 1991.

McCalpin, J.P., and S.L. Forman, Assessing the paleoseismic activity of the Brigham City segment, Wasatch fault zone; probable site of the next major earthquake on the Wasatch Front?, in *Summaries of Technical Reports*, vol. XXXIV, *U.S. Geol. Surv. Open File Rep., 93-195*, 485-489, 1993.

McCalpin, J.P., S.L. Forman, and M. Lowe, Reevaluation of Holocene faulting at the Kaysville site, Weber segment of the Wasatch fault zone, Utah, *Tectonics, 13*, 1-16, 1994.

Nash, D.B., Morphologic dating of degraded normal fault scarps, *J. Geol., 88*, 353-360, 1980.

Nelson, A.R., The northern part of the Weber segment of the Wasatch fault zone near Ogden, Utah, in *In the Footsteps of G.K. Gilbert: Lake Bonneville and Neotectonics of the Eastern Basin and Range Province*, edited by M.N. Machette, *Utah Geol. Min. Surv. Misc. Publ., 88-1*, 33-37, 1988.

Nelson, A. R., Lithofacies analysis of colluvial sediments--An aid in interpreting the recent history of Quaternary normal faults in the Basin and Range province, western United States, *J. Sediment. Petrol., 62*, 607-621, 1992.

Nishenko, S.P., Seismic potential for large and great interplate

earthquakes along the Chilean and southern Peruvian margins of South America: A quantitative reappraisal, *J. Geophys. Res., 90*, 3589-3615, 1985.

Nishenko, S.P., Probabilistic estimates for the Wasatch fault, in *Proceedings of the National Earthquake Prediction Evaluation Council*, June 11-12, 1991, Alta, Utah, edited by V.A. Frizzell, *U.S. Geol. Surv. Open File Rep., 92-249*, 16-19, 1992.

Nishenko, S.P., and R. Buland, A generic recurrence time distribution for earthquake forecasting, *Bull. Seismol. Soc. Am., 77*, 1382-1399, 1987.

Nishenko, S.P., and D.P. Schwartz, Preliminary estimates of large earthquake probabilities along the Wasatch fault zone, Utah, *Eos AGU Trans., 71*, 1448, 1990.

Ostenaa, D.A., Late Holocene displacement history, Water Canyon site, Wasatch fault, Utah, *Geol. Soc. Am. Abstr. Programs, 22*, 42, 1990.

Pantosti, D., D.P. Schwartz, and G. Valensise, Paleoseismology along the 1980 surface rupture of the Irpina fault: Implications for earthquake recurrence in the southern Apennines, Italy, *J. Geophys. Res., 98*, 6561-6577, 1993.

Pearson, E.S., and H.O. Hartley, *Biometrika Tables for Statisticians*, Cambridge Univ. Press, New York, 1956.

Perkins, D.M., Contagious fault rupture, probabalistic hazard, and contagion observability, in *Directions in Paleoseismology*, edited by A.J. Crone and E.M. Omdahl, *U.S. Geol. Surv. Open File Rep., 87-673*, 428-439, 1987.

Personius, S.F., A brief summary of the surficial geology along the Brigham City segment of the Wasatch fault zone, Utah, in *In the Footsteps of G.K. Gilbert--Lake Bonneville and Neotectonics of the Eastern Basin and Range Province*, edited by M.N. Machette, *Utah Geol. Min. Surv. Misc. Publ., 88-1*, 27-32, 1988.

Personius, S.F., Paleoseismic analysis of the Wasatch fault zone at the Brigham City trench site, Brigham City, Utah and the Pole Patch trench site, Pleasant View, Utah, in *Paleoseismology of Utah*, vol. 2, *Utah Geol. Min. Surv. Spec. Stud., 76*, 39 pp., 1991.

Rikitake, T., Recurrence of great earthquakes at subduction zones, *Tectonophysics, 35*, 335-362, 1976.

Savage, J.C., Probability of one or more $M>7$ earthquakes in southern California in 30 years, *Geophys. Res. Lett., 21*, 313-315, 1994.

Schwartz, D.P., Geologic characterization of seismic sources-- moving into the 1990's, in *Earthquake Engineering and Soil Dynamics II, Recent Advances in Ground-Motion Evaluation*, edited by J.L Von Thun, *Geotech. Spec. Publ. Am. Soc. Civ. Eng., 20*, 1-42, 19-88a.

Schwartz, D.P., Historical normal fault scarps--Wasatch Front and vicinity, in *Summaries of Technical Reports*, vol. XXV, *U.S. Geol. Surv. Open File Rep., 88-16*, 564-566, 1988b.

Schwartz, D.P., and K.J. Coppersmith, Fault behavior and characteristic earthquakes: Examples from the Wasatch and San Andreas fault zones, *J. Geophys. Res., 89*, 5681-5698, 1984.

Schwartz, D.P., K.L. Hanson, and F.H. Swan III, Paleoseismic investigations along the Wasatch fault zone: an update, *Utah Geol. Min. Surv. Spec. Stud., 62*, 45-49, 1983.

Schwartz, D.P., W.R., Lund, W.E. Mulvey, and K.E. Budding, New paleoseismicity data and implications for space-time clustering of large earthquakes on the Wasatch fault zone, Utah (abstract), *Seismol. Res. Lett., 59*, 15, 1988.

Shenon, P.J., Utah earthquake of March 24, 1934, *J. Wash. Acad. Sci., 25*, 508-509, 1935.

Sieh, K., M. Stuiver, and D. Brillinger, A more precise chronology of earthquakes produced by the San Andreas fault in southern California, *J. Geophys. Res., 94*, 603-623, 1989.

Stafford, T.W., Jr., and S.L. Forman, Radiocarbon and thermoluminescence dating of Wasatch faulting events, Garner Canyon, Utah, *Utah Geol. Surv. Contract Rep. 93-4*, 15 pp., 1993.

Stuiver, M., and P.J. Reimer, Extended ^{14}C data base and revised CALIB 3.0 ^{14}C age calibration program, *Radiocarbon, 35*, 215-230, 1993.

Swan, F.H., III, D.P. Schwartz, and L.S. Cluff, Recurrence of moderate to large magnitude earthquakes produced by surface faulting on the Wasatch fault, Utah, *Bull. Seismol. Soc. Am., 70*, 1431-1462, 1980.

Swan, F.H., III, K.L. Hanson, D.P. Schwartz, and P.L.K. Knuepfer, Study of earthquake recurrence intervals on the Wasatch Fault at the Little Cottonwood site, Utah, *U.S. Geol. Surv. Open File Rep., 81-450*, 30 pp., 1981a.

Swan, F.H., III, D.P. Schwartz, K.L. Hanson, P.L.K. Knuepfer, and L.S. Cluff, Study of earthquake recurrence intervals on the Wasatch fault at the Kaysville site, Utah, *U.S. Geol. Surv. Open File Rep., 81-228*, 30 pp., 1981b.

Sykes, L.R., and S.P. Nishenko, Probabilities of occurrence of large plate rupturing earthquakes for the San Andreas, San Jacinto, and Imperial faults, California, 1983-2003, *J. Geophys. Res., 89*, 5905-5927, 1984.

Taylor, R.E., *Radiocarbon Dating--An Archaeological Perspective*, Academic, Orlando, Fla. 1987.

Wallace, R.E., Profiles and ages of young fault scarps, north-central Nevada, *Geol. Soc. Am. Bull., 88*, 1267-1281, 1977.

Wallace, R.E., Degradation of the Hebgen Lake fault scarps of 1959, *Geology, 8*, 225-229, 1980.

Wallace, R.E., Faulting related to the 1915 earthquakes in Pleasant Valley, Nevada, *U.S. Geol. Surv. Prof. Pap. 1274-A*, 33 pp., 1984.

Wallace, R.E., Variations in slip rates, migration, and grouping of slip events on faults in the Great Basin province, *Bull. Seismol. Soc. Am., 77*, 868-876, 1987.

Ward, S.N., A synthetic seismicity model for the Middle America Trench, *J. Geophys. Res., 96*, 21,433-21,442, 1991.

Ward, S.N., An application of synthetic seismicity in earthquake statistics: The Middle America Trench, *J. Geophys. Res., 97*, 6675-6682, 1992.

Ward, S.N., How regularly do earthquakes recur? A synthetic seismicity model for the San Andreas Fault, *Geophys. Res. Lett., 20*, 2131-2134, 1993.

Wintle, A.G., and J. Catt, Thermoluminescence dating of soils developed in late Devensian Loess at Pegwell Bay, Kent, *J. Soil Sci., 36*, 293-298, 1985.

Working Group on California Earthquake Probabilities (WGCEP), Probabilities of large earthquakes occurring in California on the San Andreas fault, *U.S. Geol. Surv. Open File Rep., 88-398*, 62 pp., 1988.

Working Group on California Earthquake Probabilities (WGCEP), Probabilities of large earthquakes in the San Francisco Bay region, California, *U.S. Geol. Surv. Circ., 1053*, 51 pp., 1990.

Wu, S.-C., A.C. Cornell, and S.R. Winterstein, A hybrid recurrence model and its implication on seismic hazard results, *Bull. Seismol. Soc. Am., 85*, 1-16, 1995.

Youngs, R.R., F.H. Swan, M.S. Power, D.P. Schwartz, and R.K. Green, Probabilistic analysis of earthquake ground shaking hazard along the Wasatch Front, Utah, in *Assessment of Regional Earthquake Hazards and Risk Along the Wasatch Front, Utah*, edited by P.L. Gori and W.W. Hays, *U.S. Geol. Surv. Open File Rep., 87-585*, M1-M110, 1987.

Youngs, R.R., F.H. Swan, and M.S. Power, Use of detailed geologic data in regional probabalistic seismic hazard analysis: An example from the Wasatch Front, Utah, in *Earthquake Engineering and Soil Dynamics II- Recent Advances in Ground-Motion Evaluation*, edited by J.L. Von Thun, *Am. Soc. Civ. Engin. Spec. Publ., 20*, 156-172, 1988.

J. P. McCalpin, GEO-HAZ Consulting, Inc.., P.O. Box 1377, Estes Park, CO 80517. (e-mail: mccalpin@geohaz.com)

S. P. Nishenko, The Natural Hazards Center, University of Colorado, Boulder, CO 80309-0428.

(Received September 30, 1994; revised September 11, 1995; accepted September 14, 1995.)